Coordinated cerebellar climbing fiber activity signals learned sensorimotor predictions

William Heffley II[1], Eun Young Song[1], Ziye Xu[1], Benjamin Taylor[1], Mary Anne Hughes[1], Andrew McKinney[1,2,3], Mati Joshua[1,4] and Court Hull[1]

[1]Department of Neurobiology, Duke University Medical School, Durham, United States
[2]Neuroscience Department, Baylor College of Medicine, Houston, United States
[3]Duncan Neurological Research Institute at Texas Children's Hospital, Houston, United States
[4]Department of Medical Neurobiology, The Hebrew University, Hadassah Medical School, Jerusalem, Israel

Correspondence:

Dr. Court Hull
Duke University Medical School
Dept. of Neurobiology
311 Research Drive
Durham, NC 27710

Email: Hull@neuro.duke.edu
Phone: 919-613-0927

Acknowledgements:
This work was supported by grants from the NIH NINDS (5R01NS096289-02), the Sloan Foundation, and the Whitehall Foundation. We thank Dr. Lindsey Glickfeld for helpful discussions and input on calcium imaging approaches and analyses, Drs. Stephen Lisberger, Greg Field, Kevin Franks and Fan Wang for feedback on early versions of this manuscript, and members of the Hull and Glickfeld labs for input and technical assistance throughout the project.

Abstract

The prevailing model of cerebellar learning states that climbing fibers (CFs) are both driven by, and serve to correct, erroneous motor output. However, this model is grounded largely in studies of behaviors that utilize hardwired neural pathways to link sensory input to motor output. To test whether this model applies to more flexible learning regimes that require arbitrary sensorimotor associations, we have developed a cerebellar-dependent motor learning paradigm compatible with both mesoscale and single dendrite resolution calcium imaging in mice. Here, we find that CFs are preferentially driven by, and more time-locked to correctly executed movements, exhibiting widespread correlated activity within parasagittal processing zones that is governed by predictions about the outcome of movement. Together, these CF activity patterns are well-suited to drive learning based on successful movement by providing predictive instructional input that does not rely exclusively on motor errors.

Introduction

A key role of the cerebellum is to form predictive associations between sensory inputs and motor outputs. These sensorimotor predictions are critical for generating well-timed and accurate movements, and in the absence of cerebellar function, the lack of such predictive motor output severely impairs our ability to generate coordinated responses to stimuli in the external world.

Classic models posit that the cerebellum generates sensorimotor predictions according to a supervised learning rule[1-3]. According to such models, projections from the inferior olive called climbing fibers are thought to signal motor errors, thus providing information to Purkinje cells about discrepancies between the expected consequences of a motor command and subsequent sensory feedback. To correct erroneous motor output, the climbing fibers instruct heterosynaptic long-term depression[4-6] by producing powerful regenerative calcium transients[7-9] in Purkinje cell dendrites called complex spikes[10, 11]. In so doing, climbing fibers are thought to appropriately update the cerebellar forward internal model with revised sensorimotor predictions.

This error-signaling framework provides a compelling explanation for climbing fiber activity in a variety of simple behaviors, such as classical conditioning (e.g. eyeblink conditioning) and adaptation (e.g. vestibulo-ocular reflex gain changes)[12-14] paradigms. Such behaviors typically rely on a yoked relationship between unconditioned sensory input and motor output, allowing the cerebellum to utilize signals from hardwired pathways to drive learning. Hence, the climbing fibers can instruct learning by responding to an unconditioned stimulus (e.g. periocular eye puff or retinal slip) that produces the same movement requiring modification (e.g. eyelid closure or eye movement).

However, many forms of motor learning do not involve modifications to motor programs linked directly to an unconditioned stimulus and response. Instead, the correct association between sensory input and motor output must be learned through experience, and the sensory information necessary for learning may have no direct relationship to the movement that requires modification. Such abstract associations necessitate that learning cannot be achieved by input from hardwired sensorimotor pathways alone. Under such conditions, where an unconditioned stimulus and response alone does not contain sufficient information to guide learning, it is unclear whether the current model of supervised error signaling can account for either climbing fiber activity or the cerebellar contribution to learning.

To test how the climbing fiber system is engaged under conditions where the sensory and motor signals necessary to drive learning are not innate, we have established a cerebellar-dependent behavioral paradigm compatible with population level *in vivo* calcium imaging, optogenetic and electrophysiological approaches. Using this paradigm, we reveal two key features of cerebellar climbing fiber (CF) driven complex spiking. First, we find that complex spiking cannot be accounted for by a simple error-based supervised learning model. Instead, complex spiking can signal learned, task specific predictions about the likely outcome of movement in a manner well suited for flexible control of complex motor behaviors. Second, population level recordings reveal that while complex spiking is correlated within and across parasagittal zones, these correlations also depend on behavioral context. While previous measurements have shown increased correlations in complex spiking in response to sensory input or motor output[15-18], and have suggested an important role for synchrony in downstream processing and motor learning[19], our results reveal that such modulation can vary for identical movements depending on behavioral relevance. Hence, these data reveal key features of cerebellar CF activity that differ significantly from classically studied cerebellar behaviors, and suggest an extension to current models of cerebellar learning in order to account for the role of complex spiking in tasks that require abstract sensorimotor associations.

Results:

To determine the conditions under which climbing fiber driven complex spiking occurs during a motor learning regime that requires an arbitrary sensorimotor association, we first designed an appropriate task. An important feature of the task design is to specifically engage neurons near the dorsal surface of the cerebellum, thereby allowing for visualization of complex spikes at the population level via calcium imaging. Hence, we used optogenetics to functionally map the midlateral dorsal surface of the mouse cerebellum according to the motor output produced by spatially defined populations of Purkinje cells (PCs). To do so, we expressed Archaerhodopsin (Arch) using a transgenic approach (methods) in cerebellar PCs (Fig. 1A), and

108 used an external fiber coupled laser to transiently suppress PCs near the dorsal surface of the
109 cerebellum (Fig. 1B). Consistent with previous work[20], we identified a population of superficial
110 PCs in lobule simplex capable of driving ipsilateral forelimb movements either during optogenetic
111 silencing with Arch or following a brief train of electrical simulation (Fig. 1, Supp. Fig. 1, Supp.
112 Movie 1). *In vivo* single unit recording confirmed that our optogenetic stimulation was effective in
113 silencing superficial PCs at the threshold for driving forelimb movement (~20 mW) up to a depth
114 of 500 μm (Fig. 1B).
115
116 **A cerebellar dependent sensorimotor association learning task**
117 Based on these results, we designed a sensorimotor association task involving forelimb
118 movement, with the rationale that the cerebellar contribution to learning in such a task should
119 necessarily involve the PCs capable of driving such movements. This task contains two discrete
120 phases; one where motor output is reactive ('cue reaction'), and another where motor output
121 becomes predictive with learning ('cue prediction'). In both task variations, head restrained, water
122 deprived mice are trained to self-initiate trials by depressing a lever, and to release the lever in
123 response to a visual cue (Fig. 1C,D).
124 In the cue reaction task, trial-to-trial variability in the timing of the visual cue (Fig. 1E,G-
125 "random cue delay") is imposed to necessitate that mice employ reactive forelimb responses. In
126 this regime, lever release reaction times are reflective of the latency for sensory integration[21] and
127 remain constant throughout each session (ΔRT = 1.1 $\pm$ 9.3 ms, n=26 sessions, 7 mice, Supp.
128 Movie 2).
129 In the cue prediction task, the visual cue is presented with the same delay on every trial.
130 In this regime, mice learn to predict the timing of the cue and adjust their motor responses to more
131 closely approximate the time of cue (Fig. 1F,G, ΔRT 500ms cue delay = 154.5 $\pm$ 13.6 ms, n=44
132 sessions, 10 mice). Moreover, learning occurs within a single training session (90 min., 309-700
133 trials), is retained across days (Supp. Fig. 2A), and can be extinguished by returning mice to the
134 cue reaction paradigm (Supp. Fig. 2C,D). In addition, we find that learning depends on the
135 duration of the cue delay: maximal learning occurs at short cue delays (e.g. 500 ms) and little or
136 no learning occurs for cue delays greater than 1.5 seconds (Fig. 1H; one-way ANOVA, main effect
137 of cue delay, $p = 4.8\times10^{-6}$. Post hoc comparison to cue reaction: 500 ms, $p=1.9\times10^{-11}$, 1 s,
138 $p=8.4\times10^{-11}$, 1.5 s, p=0.359, 2 s, p=0.005). This dependence on a short interval delay is consistent
139 with the temporal characteristics of canonical cerebellar-dependent sensorimotor associative
140 learning[22].
141 To test whether animals adjust the timing or kinematics of their forelimb movement to
142 predict the timing of the visual cue, we measured lever kinematics during a subset of learning
143 sessions. Alignment of the lever trajectory to the onset of the cue revealed that animals altered

144 the time of lever release, releasing the lever sooner in anticipation of the visual cue (Fig. 1I; 20%
145 rise time occurs 116 ± 18 ms earlier, p = $1.2x10^{-5}$, paired t-test). However, despite substantial
146 variability in the kinematics of release (Supp. Fig. 3), independent alignment of both press and
147 release demonstrated that there was no change in movement kinematics across learning
148 sessions (Fig 1I-J; First 1/3 of session 20-80% release rise time= 18.9 ± 0.6 ms, last 1/3 of session
149 = 19.3 ± 0.8 ms; p=0.513, paired t-test), indicating that mice release the lever sooner but with the
150 same kinematics after learning.

151 To test the necessity of the lobule simplex for this learning, we first locally applied lidocaine
152 in order to block spiking in cerebellar cortical neurons, including PCs. However, consistent with
153 the critical tonic inhibition PCs provide to the deep cerebellar nuclei, we observed significant motor
154 deficits including slowed movement, dramatically fewer initiated trials, and dystonic limb
155 contractions (not shown). Thus, this manipulation was not appropriate to define the necessity of
156 lobule simplex in our task.

157 To avoid significant impairment of motor output, we next used a pharmacological
158 manipulation to selectively disrupt excitatory synaptic transmission in lobule simplex without
159 abolishing the spontaneous pacemaking of PCs. For these experiments, we optimized
160 concentrations of the excitatory synaptic transmission blockers NBQX (300 μM), CPP (30 μM)
161 and MCPG (30 μM) to avoid visible impairment of motor output, and then tested this cocktail
162 during behavior. Following local drug application to lobule simplex (methods), mice retained the
163 ability to release the lever in response to the visual cue, maintaining stable kinematics across
164 sessions (Fig. 2A,B) that were not different from control sessions (Fig. 1I,J, and Supp. Fig. 3;
165 Press: control range = 28.97 ± 2.5 ms, NBQX range = 25.33 ± 1.9 ms, p=0.2612; Release: control
166 range = 6.16 ± 1.2 ms, NBQX range = 4.13 ± 1.06 ms, p=0.2215, unpaired t-test). These data
167 suggest that motor output was not significantly impaired as a result of this pharmacological
168 manipulation. However, despite stable movement kinematics, learning was severely impaired
169 when the cue was presented with a constant 500 ms delay (Fig 2A,C,D) (NBQX ΔRT with 500 ms
170 cue delay = 48.8 ± 26.7, control ΔRT with 500 ms cue delay = 154.5 ± 13.6 ms, ΔRT with cue
171 reaction = 1.1 ± 9.3, unpaired t-test NBQX vs control 500 ms p=$4.6x10^{-4}$, unpaired t-test NBQX
172 vs control cue reaction p=0.05). Acute single unit PC recordings during drug application revealed
173 that this manipulation significantly reduced complex spike rates, consistent with a reduction in the
174 amplitude of postsynaptic glutamatergic currents produced by climbing fiber input (control 0.60 ±
175 0.07 Hz, NBQX/CPP/MCPG 0.27 ± 0.04 Hz, n = 9, p=$8.5x10^{-4}$, paired t-test, Supp. Fig. 4). We
176 also found a modest reduction in simple spiking, consistent with reducing excitatory synaptic input
177 from the mossy fibers and parallel fibers (control 66.8 ± 17.8 Hz, NBQX/CPP/MCPG 45.9 ± 13.0
178 Hz, n = 8, n = 9, p=0.36, paired t-test). Hence, these data support that hypothesis that synaptic

179 transmission in lobule simplex is necessary for predictive sensorimotor learning to occur in the
180 cue reaction phase of our task.
181
182 **Complex spiking is not driven by motor errors in a voluntary motor learning task**
183 To test how the olivary system is engaged in this behavior, we imaged climbing fiber
184 evoked calcium signals in mice performing the cue reaction phase of our task. In this regime, all
185 sensorimotor signals are in place to drive learned, predictively timed forelimb movements, but no
186 learning can occur due to the variable cue timing (Fig. 1G,H). Hence, we can test what task
187 features drive complex spiking in a stable regime. We began by using a single photon microscope
188 to image populations of PCs virally expressing GCaMP6f (methods). Image segmentation in a
189 subset of experiments with the most superficial GCaMP expression revealed structures consistent
190 in size and shape with PC dendrites in cross section (Supp. Fig. 5). Calcium transients in these
191 structures occurred at 0.5 $\pm$ 0.01 Hz, consistent with the baseline rate of complex spiking we
192 measured with single unit electrophysiology (Supp. Fig. 5). These results are also consistent with
193 several *in vivo* calcium imaging studies using a variety of GCaMP variants showing that PC
194 responses are dominated by the large dendritic calcium transients produced by climbing fiber
195 driven complex spikes[15-18, 23-28].
196 We next identified regions of interest, defined by the expression pattern of GCaMP in each
197 animal, that were restricted to the region within lobule simplex capable of driving ipsilateral
198 forelimb movements (methods). Consistent with the role of this region in the control of forelimb
199 movements, we observed task modulated PC calcium transients associated with the timing of
200 lever press and release, with the largest modulation at the time of lever release (Fig. 3A-C).
201 Surprisingly, when we segregated trials according to outcome, we observed significantly larger
202 calcium transients associated with lever releases when animals correctly released the lever in
203 response to the visual cue as compared to trials where lever release occurred prior to the cue
204 (Correct = 0.156 $\pm$ 0.023 $\Delta F/F$; Early = 0.092 $\pm$ 0.018 $\Delta F/F$, n=17 sessions, 10 animals, $p=4.60\times10^{-}$
205 ^{5}, paired t-test). These enhanced responses were distributed widely across dorsal, superficial
206 lobule simplex, and were consistent across sessions and animals (Fig. 3D). The same pattern of
207 enhanced complex spiking on correctly timed lever releases was observed in the cue prediction
208 task as measured by single unit PC electrophysiological recordings (Supp. Fig. 6). Thus, in this
209 motor task, our data suggest that complex spikes occur preferentially on correctly timed
210 movements, and not motor errors.
211 There are many differences between the correct and early release trials that could
212 contribute to the observed outcome-dependent difference in complex spiking. One possible
213 difference between trial types could be the kinematics of the forelimb movement. Hence, in a
214 subset of our experiments, we measured movement kinematics by comparing lever trajectories

215 on correct and early release trials (Fig. 4A-B). These data revealed closely matched movement
216 kinematics between correct and early lever release trials (Press: correct = 26.8 ± 1.6 ms, early =
217 25.1 ± 1.3 ms; Release: correct = 18.9 ± 0.8 ms, early: 22.1 ± 1.5 ms, n=14 sessions).
218 Another difference between correctly timed and early lever releases is that reward is only
219 delivered on correct trials, and this results in extended licking. Indeed, we find that lick rates were
220 significantly higher and prolonged on correct trials (Fig. 4C; correct = 10.5 ± 0.7 Hz, early = 1.5 ±
221 0.4 Hz, $p=3.74x10^{-9}$, paired t-test, n=9 animals, 15 sessions). Moreover, in some recording
222 sessions we observed a late, sustained calcium transient that occurred during licking (Fig. 4D).
223 However, we found no correlation between the mean early, peak calcium transients and mean
224 lick rates across trial types (Fig. 4E,F; Correct $R^2=0.182$, p=0.11; Early $R^2=5.97x10^{-5}$, p=0.98,
225 ANOVA) or within sessions across trials of each type (Fig. 4G; Correct ρ = -0.002 ± 0.028, p=0.93;
226 Early $\rho = 0.054 \pm 0.113$, p=0.65, one sample t-test; Supp. Fig. 7D; Correct ρ = 0.0053 ± 0.0019,
227 p=0.544; Early $\rho = 0.0912 \pm 0.0048$, p=0.428, n=447 dendrites, one sample t-test). Thus, we
228 conclude that the enhanced responses as measured by the early peak calcium transient on
229 correctly timed lever releases are not due to differences in forelimb movement kinematics or
230 licking, but are instead linked to the context of the movement.
231
232 **Behavioral context determines the probability and synchrony of complex spiking**
233 To investigate the dynamics of complex spiking at the single cell level, we used video-rate
234 two-photon microscopy to image the dendrites of PCs during behavior. Using this approach, we
235 isolated the dendrites of individual PCs[24] (Fig. 5, Supp. Figs. 5, 8), and measured both
236 spontaneous and task-evoked calcium transients. As with the single photon imaging experiments,
237 spontaneous calcium transients measured during inter-trial intervals occurred at a rate of 0.61 ±
238 0.01 Hz, consistent with our electrophysiological measurements of spontaneous complex spiking
239 (Supp. Fig. 5E,F). The two-photon data also replicated the main finding that the mean calcium
240 transients were significantly larger on correct release trials within individual PC dendrites (Correct
241 = 0.101 ± 0.004 $\Delta F/F$; Early = 0.035 ± 0.002 $\Delta F/F$, n=1146 dendrites, $p=9.79^{-76}$, paired t-test) (Fig.
242 5A,B). Moreover, lever releases that were rewarded but occurred too fast to be responses to the
243 visual cue (reaction times less than 200 ms) produced calcium transients that were significantly
244 smaller than those produced by correct lever release trials ('Too fast' 0.029 ± 0.002 $\Delta F/F$, $p=3.91^{-}$
245 ^{104}, paired t-test) and not significantly different from responses on early release trials (p=0.086).
246 Hence, these data support the analysis in Figure 4 that the enhanced complex spiking on correct
247 trials is not due to licking or reward per se.
248 In addition to larger mean responses across trials, population level analysis revealed that
249 more PCs were driven on correct release trials (Fig 5C). Of the total population of PCs that
250 responded to any lever press or release (1146 of 1302), most (88%) PCs exhibited complex

251 spikes on correct release trials, whereas less than half (41%) responded during early lever
252 releases (Fig. 5D, *top*). Approximately half (48%) of PCs exhibited complex spikes in response
253 to lever press (Fig. 5D, *bottom*). The increased number of active dendrites on correct trials is
254 unlikely to be a thresholding artifact, since there was no significant difference in the average
255 response amplitude of correct-only and correct+early responsive dendrites to correct trials
256 (Correct only 0.112 ± 0.006 ΔF/F, n=578; Correct + Early 0.119 ± 0.005 ΔF/F, n=457 dendrites,
257 p=0.44 unpaired t-test). These data also indicate that the measured increase in number of active
258 dendrites is not due to contamination of fluorescent signals from neighboring dendrites. Hence,
259 these single dendrite measurements explain our single photon results by demonstrating that both
260 more PCs exhibit complex spikes on correct trials, and those dendrites that exhibit complex spikes
261 in response to both trial types have larger mean calcium transients on correct trials.

262 The difference in the average release-evoked response on correct versus early trials may
263 be due to a difference in the amplitude of the calcium transients on each trial. For instance,
264 complex spikes are not "all-or-none" events[29], and the number of spikelets can vary from event to
265 event[30-32], altering the size of the evoked calcium transient[33]. Thus, we extracted single trial
266 events associated with lever releases across trial types, and compared these with each other and
267 to the spontaneous calcium transients. However, this analysis revealed no significant difference
268 between the amplitude of calcium transients evoked on single trials in response to either correct
269 or incorrect lever releases (Correct 0.266 ± 0.004 ΔF/F n=19,550 events, Early 0.263± 0.004 ΔF/F
270 n=9,167 events), and between movement-evoked and spontaneous activity (Spontaneous 0.272
271 ± 0.004 ΔF/F n=286,964 events) (p=0.17, one-way ANOVA) (Fig. 5E). Thus, if there are variable
272 numbers of evoked spikelets across trials, such differences are not systematically correlated with
273 either trial outcome or task engagement. Moreover, the equivalent amplitude of lever-evoked and
274 spontaneous events suggests that the majority of the measured signal is from calcium influx due
275 to complex spiking, and is not substantially influenced by additional input from the parallel fibers.
276 Indeed, the size and shape of our segmented ROIs is consistent with several studies showing
277 that complex spikes produce a calcium signal throughout the entire PC dendrite[7, 9], whereas
278 parallel fiber calcium signals are much smaller and confined to isolated regions of spiny dendritic
279 branchlets[34-37].

280 To assess how equivalent single event responses can produce larger mean responses on
281 correct trials, we generated a peristimulus time histogram of complex spike events for each trial
282 type aligned to the time of release (Fig. 6A). This analysis revealed a significantly enhanced
283 complex spike rate at the time of lever release for trials when movement was correctly timed (Fig.
284 6A,B; correct spike rate=2.04 ± 0.05 Hz, early spike rate= 1.33 ± 0.04 Hz, $p=8.14\times10^{-15}$, n=1146
285 dendrites, paired t-test). In addition, complex spiking on correct trials in single PC dendrites
286 occurred with shorter latency (Fig 6C; correct latency=35.86 ± 1.19 ms, early latency=46.49 ±

287 1.25 ms, $p=2.65x10^{-11}$, n=1146 dendrites, paired t-test) and less temporal jitter across trials (Fig
288 6D; correct jitter (S.D of latency) = 53.79 ± 1.39 ms S.D., early jitter 95.16 ± 1.88 ms S.D.,
289 $p=6.16x10^{-45}$, n=1146 dendrites, unpaired t-test). Notably, these measures of jitter are likely to
290 be an overestimate since our measure of event time is limited by our sampling interval (33 ms),
291 and the true onset might have occurred between samples. However, when accounting for the
292 overall spontaneous event rate of ~1 Hz, the 50 ms jitter of events on correct trials is comparatively
293 precise.
294 These results also suggest the possibility of enhanced synchrony at the population level
295 on correct release trials. Indeed, in some sessions, we measured enhanced population
296 synchrony across dendrites (Fig 6E; 13 out of 30 sessions have significantly elevated synchrony
297 on correct trials, open circles, $p<0.05$ for each session, mean across the population is not
298 significant, p=0.098, paired t-test.). However, in many experiments, we observed no such
299 increase in population synchrony on correct trials. We thus considered the possibility that
300 enhanced synchrony was location specific, and might obey spatial structure that was not well
301 demarcated at the scale of the field of view in our two-photon experiments.
302
303 **Context determines correlated population activity at the mesoscale level**
304 To investigate whether correlated complex spiking was spatially organized, we returned
305 to single photon imaging and analyzed experiments that exhibited widespread GCaMP
306 expression across superficial lobule simplex (n=5 animals, 7 sessions). Using an unsupervised,
307 iterative pixel-clustering approach[26] (methods), we first assessed correlations between pixels
308 across all trials (Fig. 7A). Despite non-uniform, unpatterned GCaMP expression, this analysis
309 revealed spatial patterns of correlated activity that were organized across parasagittal bands
310 oriented in the rostro-caudal axis. These bands were 221 ± 15 μm wide on average across 39
311 measured zones, consistent with previous anatomical and physiological measurements of
312 cerebellar microzones[38, 39]. Hence, these data support the longstanding hypothesis that the
313 anatomical pattern of climbing fiber projections into the cerebellar cortex establishes functionally
314 distinct parasagittal processing modules.
315 To test how complex spiking is modulated during behavior within and across parasagittal
316 zones, we divided trials according to outcome and analyzed brief epochs surrounding the time of
317 lever release (Fig. 7B). While this analysis lacks the fine temporal resolution of the two-photon
318 event based analysis in Figure 6, it nonetheless revealed that activity amongst pixels within a
319 zone exhibited higher correlations for most zones on correct lever release trials as compared to
320 early release trials ($r_{correct}$ = 0.77 ± 0.01, r_{early} = 0.69 ± 0.017, $p = 1.60x10^{-5}$, n=39 clusters, paired
321 t-test) (Fig. 7C). Because higher spike rates can cause larger correlations, we tested whether
322 the higher complex spike rates on correct trials could account for the higher correlations. While

323 increased complex spiking did produce larger correlations, early release trials still had weaker
324 correlations than correct release trials across equivalent activity levels as assessed by linear fits
325 to bootstrapped distributions paired from each trial type (methods) (Fig. 7D). Hence, the
326 enhanced correlations on correct trials are not an artifact of enhanced complex spike rates on
327 correct trials. We also found enhanced correlations between neighboring and non-neighboring
328 zones on correct lever release trials (Fig. 7E,F) (Correct $r_{neighboring}$ = 0.69 ± 0.03, n=31 cluster
329 pairs, p=0.004 vs early, Correct $r_{non\text{-}neighboring}$ = 0.65 ± 0.03, n=50 cluster pairs, $p=6.2\times10^{-12}$ vs
330 early, paired t-test). However, these cross-zone correlations were significantly lower on average
331 than those within zones (within zone vs neighboring, p=0.004; within zone vs. non-neighboring
332 $p=3.4\times10^{-4}$, unpaired t-test). Hence, these data reveal a precise spatial organization of climbing
333 fiber activity, with highly correlated complex spiking within parasagittal zones that is task specific,
334 differing for movements with the same kinematics depending on behavioral context.
335
336 **Complex spiking signals learned sensorimotor predictions**
337 Our data suggests that complex spiking does not signal motor errors in this behavioral
338 paradigm. Instead, our results are consistent with the possibility that the climbing fibers signal
339 either 1) correctly timed motor output, 2) a temporal-difference (TD) prediction error driven by the
340 unexpected visual cue that instructs lever release and predicts upcoming reward delivery, or 3)
341 an expectancy signal related to the probable outcome of movement. To distinguish between these
342 possibilities, we took advantage of the temporal structure of the task, wherein the probability of
343 cue appearance, and thus reward delivery, increases with lever hold time (i.e. the hazard function
344 is not flat). Thus, we tested whether complex spiking depends on lever hold time for correct and
345 early lever releases.
346 We find that while complex spiking is independent of lever hold time for correctly timed
347 movements (1P: ρ = -0.07, p=0.76, n=17 sessions ; 2P: correct ρ = -0.01, p=0.98 n=30 sessions;
348 Fig. 8 A,B), there is a strong positive relationship between lever hold time and complex spiking
349 for early lever releases across both single and multiphoton imaging sessions (1P: 0.91 $p<1.0\times10^{-}$
350 ^{16}, n=17 sessions; 2P: early ρ = 0.90, $p=4.58\times10^{-6}$, n=30 sessions ; Fig. 8 A,B). The elevated
351 complex spiking associated with longer lever hold times is due to both an increase in spiking at
352 the time of lever release (Window 1: short duration early $\Delta F/F = 0.03 \pm 9.55\times10^{-4}$, long duration
353 early $\Delta F/F$ = 0.04 ± 0.00, $p=3.84\times10^{-10}$, n=1146 dendrites, paired t-test; Figure 8C), and an
354 additional late response not present on short duration early release trials (Window 2: short
355 duration early $\Delta F/F$ = 0.04 ± 0.00, long duration early $\Delta F/F$ = 0.07 ± 0.00, $p=1.33\times10^{-25}$; Figure
356 8C). The late response occurred on single trials and within individual dendrites, indicating that it
357 was not generated by a diversity of response timings across trials or by a separate population of
358 PC dendrites (Fig. 8 D). In addition, the late response did not correlate with an increase in licking

359 on long duration trials, and occurred approximately 200 ms after lever release when lick rates
360 began to decrease and reward delivery was no longer possible (Fig 8 H,I). These results are
361 consistent with an expectancy model, where complex spiking signals both an initial prediction
362 about movement outcome and a readout of whether the initial prediction was violated. In this
363 model, an initial prediction accompanies lever release that depends primarily on cue presentation
364 (Window 1: long duration correct $\Delta F/F = 0.07 \pm 0.00$, long duration early $\Delta F/F = 0.04 \pm 0.00$, $p =$
365 3.16×10^{-7}, n=1146 dendrites, paired t-test). While the visual cue provides the strongest prediction
366 of trial outcome, trial duration also contributes to expectation according to the task structure. In
367 the case that initial expectation is unmet, the climbing fibers also signal this unexpected outcome
368 through an increase in spiking.
369 To further test this model, we performed a second set of experiments to probe the role of
370 violated expectations in driving complex spiking. In these experiments, we omitted reward
371 delivery on 20% of correctly timed lever releases (Fig. 8 J-N). Consistent with the cue
372 appearance establishing expectation at the time of lever release, both rewarded and omission
373 trials resulted in calcium transients that were nearly equivalent at the time of lever release
374 (Window 1: rewarded = 0.07 ± 0.01, omission = 0.07 ± 0.01 ; $p=0.04$, n=81 dendrites, paired t-
375 test; Figure 8L). However, omission trials resulted in an additional, late response at the time when
376 lick rates began to decrease and reward delivery was no longer possible (Window 2: rewarded =
377 0.06 ± 0.01, omission = 0.08 ± 0.01; $p=2.54 \times 10^{-9}$, n=81 dendrites, paired t-test; Figure 8M). The
378 timing of this late response was similar to the late response following long duration early releases,
379 and was present on single trials and within individual dendrites (Figure 8J,N). Hence, these
380 experiments support the hypothesis that climbing fibers can both signal and evaluate predictions
381 about the likely outcome of movements.
382
383 **Discussion**
384 We have established a sensorimotor association task that involves PCs near the dorsal
385 surface of lobule simplex. This behavior has several hallmarks of cerebellar learning, including a
386 dependence on short delay intervals for generating the learned sensorimotor association and the
387 requirement for excitatory synaptic transmission in the cerebellar cortex. In this behavior,
388 however, climbing fibers do not signal erroneous motor output as described by classical models
389 of supervised learning. Specifically, we demonstrate that climbing fiber driven complex spiking
390 occurs with higher probability, shorter latency, and less jitter when movement is correctly timed.
391 Our data support the hypothesis that these enhanced climbing fiber responses are related
392 to the predicted outcome of movement, which in this behavior constitutes delivery of a water
393 reward. Evidence supporting this model is threefold: First, the highest probability of complex
394 spiking occurs on correctly timed lever releases when the visual cue instructs behavior and thus

395 a high reward expectation. Second, complex spiking is modulated by the temporal features of the
396 task that dictate expectation. Specifically, complex spiking in response to lever release increases
397 with increasing hold duration, matching the increased likelihood of reward as trial length
398 increases. Third, complex spiking is also driven when the expectation of reward is violated, both
399 when the reward is omitted on correctly executed movements and on longer hold duration early
400 releases when a correct outcome of lever release is more probable. Together, these experiments
401 suggest that climbing fibers carry instructional signals that both predict and evaluate the expected
402 outcome of movement. Such responses are consistent with the known role of cerebellar circuits
403 in generating predictive motor output, and we suggest that they could thus provide a substrate for
404 generating and testing the type forward models that have long been hypothesized to govern
405 cerebellar processing.

406 The climbing fiber activity observed in response to violated expectations has some
407 similarities to the motor error signals seen in classic cerebellar behaviors. However, in our
408 behavioral paradigm, we emphasize that these climbing fiber responses do not reflect motor
409 errors: the movements on trials in which rewards are omitted are identical to those in which
410 rewards are earned. Thus, these results indicate that the climbing fibers can respond differentially
411 to the very same movement according to its expected outcome. These context-specific climbing
412 fiber responses may be due to aspects of our task design. The behavior described here differs
413 from most cerebellar dependent learning regimes in that the movement requiring modification
414 (lever release) is not directly related to an unconditioned stimulus (reward) or response (licking).
415 As a consequence, the cerebellum cannot harness sensorimotor input from hardwired pathways
416 to enable learned changes in motor output. Instead, the necessary forward model must define
417 and evaluate the relationship between a neutral visual stimulus, a forelimb movement, and
418 reward.

419 It remains unclear whether the climbing fiber activity that enables such a forward model is
420 generated at the level of the olive, or if it is inherited from upstream brain regions such as the
421 neocortex, colliculus, or elsewhere. However, evidence suggests that the olive may have access
422 to different information depending on task requirements. Anatomical and physiological work in the
423 rodent has demonstrated that the pathway from the forelimb region of motor cortex to the IO is
424 independent of the pathway providing ascending sensorimotor input to the olive from the
425 periphery[40]. Such data argue that the olive has access to unique information in tasks that involve
426 a descending motor command, and further suggest that the olive may have access to diverse
427 cortical computations. Indeed, the presence of abstract task timing information in the activity of
428 the climbing fibers suggests that the olive has access to higher-order signals. In support of this
429 view, evidence from a different forelimb movement task in non-human primates that also requires
430 an abstract sensorimotor association has shown similar climbing fiber responses[41]. Specifically,

431 this study demonstrated that complex spikes can signal both the predicted destination of reaching
432 as well as deviations from the expected destination.

433 Importantly, the climbing fiber activity patterns described here are appropriate to drive
434 motor learning under conditions that require flexible sensorimotor associations. Specifically, the
435 higher probability complex spiking and enhanced correlations at the population level are both
436 context dependent and spatio-temporally organized. At the population level, our single photon
437 imaging of cerebellar complex spiking has revealed correlated activity within parasagittal bands
438 of approximately 200 μm, likely corresponding to "microzones"[16, 26, 39, 42-46]. Because PCs across
439 microzones can respond to different sensorimotor input, and have different spiking[47] and
440 synaptic[48] properties, these zones are thought to constitute discrete computational units in the
441 cerebellum. Recent measurements have revealed that complex spiking in microzones can
442 become more synchronous during both motor output[18] and sensory input[15, 16, 27]. Our population
443 imaging results provide a fundamental extension to this idea by demonstrating that correlated
444 complex spiking within parasagittal zones is not simply enhanced by sensorimotor input, but
445 rather can be enhanced for the same action according to behavioral context. Precisely timed
446 spiking across a large population of nearby PCs that receive common parallel fiber input and
447 converge to the same DCN neurons would provide an ideal substrate to maximize the impact of
448 plasticity. However, other circuits could also play a role in learning. In particular, complex spiking
449 can robustly inhibit nuclear neurons[49, 50], and enhanced climbing fiber synchrony would magnify
450 this effect via convergence of simultaneously active PC axons in the DCN[51]. Because
451 synchronous inhibition has been shown to play a key role in synaptic plasticity at nuclear neuron
452 synapses[52, 53], correlated complex spiking across populations of nearby PCs could place the DCN
453 as the central site of learning under such conditions[54]. In either case, we note that the climbing
454 fiber responses following correct lever releases are well-timed to promote learning in our cue
455 prediction task by instructing movements that more closely approximate earliest time of reward
456 delivery.

457 Finally, it is notable that ours are not the first results to suggest alternate learning rules
458 instructed by climbing fiber activity. Recently, conditioned eyeblink learning data has pointed
459 toward climbing fibers implementing temporal difference (TD) reinforcement learning rule by
460 signaling sensory prediction errors in order to instruct motor learning[55]. Because we do not
461 observe evidence of negative prediction errors on reward omission trials or long duration early
462 release trials, our results are incompatible with this model as strictly interpreted. Instead, our data
463 show some similarities with the type of unsigned prediction signals observed in serotonergic[56]
464 and other neurons[57, 58] that have been also thought to enable associations between unexpected
465 outcomes and novel cues[59]. Evidence for both models can often be found in neural activity within
466 the same brain region, and it has been suggested that TD and unsigned prediction mechanisms

467 may in fact be linked, and act together to promote learning[60]. Hence, as has been done in other
468 brain regions, it will be necessary to systematically vary task parameters such as the valence of
469 instructional stimuli and the requirements for learned associations in order to resolve how the
470 cerebellum implements discrete learning rules according to task demands. For the present, the
471 results described here provide an important new demonstration that complex spiking can signal
472 learned, task specific information necessary for flexible control of complex motor behaviors in a
473 manner that does not depend exclusively on motor errors.
474
475
476
477
478
479 **Author Contributions**
480 WH, ES, AM, MJ, and CH designed experiments, WH, ES, AM, BT, MAH, and MJ conducted
481 experiments, WH, ES, ZX, BT, AM, MJ, and CH analyzed data, and CH wrote the manuscript.
482
483 **Figure Legends**
484
485 **Figure 1**. Cerebellar sensorimotor task for head-fixed mice. Ai) Confocal image of a sagittal
486 section from PCP2-Cre x Arch mouse showing expression of the inhibitory opsin Arch in PCs at
487 low (left) and high (right) resolution. ML; molecular layer, PCL; Purkinje cell layer, GCL; granule
488 cell layer. Aii) Schematics of a cranial window implanted over lobule simplex (left) and
489 configuration for optogenetic stimulation (right). Bi) *Left*, representative single unit recording of
490 PC simple spike raster (top) and spike rate histogram (bottom) aligned to onset of Arch activation.
491 *Right*, Location of the stimulation sites that evoked ipsilateral forelimb movements (green). Bii)
492 Average normalized firing rates from superficial (top) or deep (bottom) PCs at low (left) or high
493 (right) stimulation powers (n=5 mice; 10-20 mW – superficial: n=6 cells; deep: n=5 cells; 30-50
494 mW – superficial: n=10 cells; deep: n=4 cells). Note that the lower powers used to map motor
495 responses were only sufficient to strongly suppress neurons above 500 μm. C) Schematic of
496 configuration of behavioral task. Head-fixed mice were trained to release a lever in response to a
497 visual cue, with reward delivered immediately upon correctly timed movement. D) Schematic of
498 trial structure. The delay between lever press and release cue was either randomized (cue
499 reaction) or constant (cue prediction) from trial to trial. E) Average reaction time (from cue onset)
500 as a function of trial number for an example cue reaction session. Each point is the average of 5
501 trials. F) Same as E, for a cue prediction session. G) Summary of reaction times for all cue
502 prediction sessions with a 0.5 s cue delay (gray; n=44 sessions, 10 mice) and all cue reaction

503 sessions (black; n=26 sessions, 7 mice). Error bars are ±SEM across sessions. H) Average
504 change in reaction time from the beginning to the end of cue prediction and reaction sessions
505 (methods). I) *Top*, average lever kinematic traces from an example 0.5 s cue prediction session
506 aligned to the cue show that lever releases occur sooner in the last 1/3 of trials (black) as
507 compared to the first 1/3 of trials (gray). Shaded area is ±SEM across trials. *Bottom,* same
508 example session as above aligned separately to press and release showing no difference in
509 kinematics from beginning (gray) to end (black) of the session. J) Summary of average lever
510 release times (20-80% rise time) across sessions (n=15 sessions, 4 mice)
511
512 **Figure 2**. Learning requires synaptic transmission in lobule simplex. A) Average lever kinematic
513 traces from an example 0.5 s cue prediction session after application of NBQX (300 μM), CPP
514 (30 μM) and MCPG (30 μM). *Top*, traces aligned separately to press and release showing no
515 difference in kinematics from beginning (blue, first 1/3 of trials) to end (black, last 1/3 of trials) of
516 the session. *Bottom*, traces aligned to the cue show that lever releases do not occur sooner in
517 the last 1/3 of trials (black) as compared to the first 1/3 of trials (blue). Shaded area is ±SEM
518 across trials. B) Summary of average lever release times (20-80% rise time) across NBQX 0.5s
519 cue prediction sessions (n=10 sessions, 6 mice). C) Summary of all 0.5 s cue prediction sessions
520 where NBQX (n=14) CPP (n=14) and MCPG (n=8) were applied locally to LS (blue; n=6 mice)
521 compared to summary of cue reaction sessions (black; replotted from Fig 1G). D) Average
522 change in reaction time from the beginning to the end of NBQX 0.5s cue prediction sessions (blue;
523 n=10 sessions, 6 mice) compared to cue prediction and reaction sessions (replotted from Fig. 1H)
524
525 **Figure 3.** Single photon imaging during cue reaction sessions. A) Example ΔF/F single trial
526 timecourses for a correctly timed lever release (left) and an early lever release (right). RW =
527 reward, delivered immediately on correct release. B) Field of view (images separated by 100 ms)
528 showing the average fractional change in fluorescence aligned to lever release for correct (top)
529 and early (bottom) trials from an example session (same session as example from A. C) Calcium
530 transient timecourses averaged across trials from the experiment in A,B) for correct (black) and
531 early trials (red). Error bars are ±SEM across trials. D) Summary of the average peak calcium
532 transients (measured on single trial basis, methods) for all correct and early trials across sessions
533 (n=10 animals, 17 sessions). Colors represent different animals, and each point represents an
534 imaging session. Note that all points lie below the diagonal. *Inset*, schematic of ROIs for all
535 sessions. Outline color corresponds to mouse from scatter plot, and fill color indicates imaging
536 depth identified by post-hoc histology.
537

538 **Figure 4**. Lever dynamics and licking do not explain differences in complex spiking across trial
539 types. A) Average lever kinematics from a representative cue reaction session for correct (black)
540 and early (red) trials aligned to threshold crossing for both press and release. B) Summary of rise
541 times for press (left) and release (right) on correct and early trials across sessions (n=14 sessions,
542 3 mice). C) Average timecourse of licking for correct (top) and early (bottom) release trials across
543 sessions (n=15 sessions, 9 mice). Error bars are ±SEM across sessions. D) Two example
544 sessions illustrating the relationship between release-evoked calcium transients (black and red
545 lines) and licking (blue bars) for correct (left) and early (right) release trials. E) Summary of the
546 relationship between lick rates and the magnitude of fluorescent transients for correct (black) and
547 early (red) release trials (n= 15 sessions, 9 mice). Error bars are ±SEM across trials. F) Summary
548 of the mean ratio of early and correct trial-evoked peak calcium transient and lick rates for the
549 same sessions in E. G) Summary of the Spearman's correlation (ρ) between lick rate and peak
550 $\Delta F/F$ on correct (black) and early (red) lever releases across trials for each session (n=8 sessions,
551 7 animals). Filled circles are mean and SEM across sessions.
552
553 **Figure 5**. Complex spiking produces larger mean response in individual dendrites and enhanced
554 population responses when movement is correctly timed. A) *Left*, average GCaMP fluorescence
555 from an example 2-photon imaging session (30 Hz acquisition rate). Scale bar = 100 μm. *Middle*,
556 pixel mask of individual PC dendrites extracted from the same session. Right, average calcium
557 responses measured from the highlighted dendrite segregated by trial event. Dotted line
558 represents time of lever press (blue) or lever release (correct: black; early: red). Shaded area is
559 ±SEM across trials. B) Left, average timecourse of calcium response for all significantly
560 responsive dendrites aligned to lever press (blue), or release (correct releases (black), early
561 releases (red), and too-fast releases (green) that occurred < 200 ms following the visual cue;
562 n=17 animals, 30 sessions, 1146 dendrites). Shaded area is ±SEM across dendrites. *Middle*,
563 summary scatter plot comparing the average peak amplitude of the calcium transient for each
564 significantly responsive PC dendrite (gray) and the average of all dendrites (red) for correct and
565 early release trials. *Right*, same as middle for correct and too fast release trials. C) Pixel masks
566 of dendrites significantly responsive to lever release on correct trials, lever release on early trials,
567 and lever press for the example session in A. Color map represents average $\Delta F/F$. D) Summary
568 across experiments of the fraction of dendrites responsive to correct lever releases vs early
569 releases (top, left), to only correct or only early releases (top, right), to lever press vs release
570 (bottom, left), and only to press or release (bottom, right). E) *Left,* average amplitude of correct
571 and early release-evoked calcium events across all dendrites normalized to the amplitude of
572 spontaneous calcium events. *Right,* mean spontaneous (gray) and correct (black) and early (red)

573 release lever-evoked calcium events across all responsive dendrites Error bars are ±SEM across
574 cells.
575
576 **Figure 6**. Complex spiking occurs with higher peak rates and greater synchrony when movements
577 are correctly timed. A) Peri-release time histogram of calcium events on correct (black) and early
578 (red) release trials (n=17 animals, 30 sessions, 1146 dendrites). Shaded area is ±SEM across
579 dendrites. B) Summary of average event rate for correct and early releases across sessions.
580 Error bars are ±SEM across dendrites. C) Same as B for average event latency relative to release.
581 D) Summary of average standard deviation (S.D.) across events within single dendrites across
582 trials. Error bars are ±SEM across dendrites. E) Same as D for measurement of S.D. across
583 dendrites within each experiment. Open circles are statistically significant for reduced correct trial
584 jitter across dendrites. Error bars are ±SEM across trials.
585
586 **Figure 7**. Complex spiking is correlated across parasagittal zones, with higher correlations on
587 correct lever releases. A) *Left*, Average GCaMP fluorescence for three example experiments.
588 ROIs from lobule simplex (white boxes) were selected for unsupervised clustering analysis (meta
589 K-means, methods). *Right*, voxels are colored according to cluster identity for each example
590 experiment. M=medial, R=rostral, C=caudal, L=lateral. Note the alignment of the clustered zones
591 along the rostro-caudal axis. B) Within cluster voxel-by-voxel correlations between correct and
592 early lever release trials from an example session in A (bottom) for each of the six identified
593 clusters (yellow). C) Summary of average correlation coefficient for all voxel pairs within an area
594 across experiments for correct and early release trials. (n=5 animals, 7 sessions, 39 clusters).
595 Colors denote clusters from the same session. Error bars are ±SEM across voxel pairs. D)
596 Summary of the relationship between peak ΔF/F and correlation coefficients for correct (black)
597 and early (red) trials. Lines are linear fits to each cluster. E) Same as C for pairs of voxels across
598 neighboring clusters. F) Same as C for pairs of voxels across non-neighboring clusters.
599
600 **Figure 8.** Complex spiking is modulated by learned sensorimotor predictions. A) Summary of
601 peak calcium transients in a 500 ms window at the time of release (methods) across all single
602 photon experiments for correct (black) and early (red) release trials binned according to hold time
603 (250ms bins). Linear fits were applied to data from each trial type (n=10 animals, 17 sessions).
604 B) Same as in A, for 2-photon imaging (n=17 animals, 30 sessions). C) Mean timecourse of
605 calcium transients for an example session divided according to early trials with hold durations of
606 < 1.0s (red) and > 3.5s (dark red). Note the late, second response for long hold duration trials. D)
607 Single trial example timecourses from an individual dendrite from the session in C). Gray bars
608 represent analysis windows for subsequent plots E-G) Summary of peak calcium transients

609 measured in the shaded windows from D for all dendrites (n=1146) according to lever hold time
610 (E,F) and trial outcome (G). H) Mean calcium transient timecourses averaged across all dendrites
611 on short and long hold early release trials. I) Mean lick rates for the subset of experiments where
612 licking was measured in H (n= 6 animals, 10 sessions)). J) Example timecourses of mean calcium
613 transients from a single session for correct (black), and reward omission (dark blue) trials. Note
614 the late, second response on omission trials. K) Single trial example timecourses from an
615 individual dendrite from the session in J. L-M) Summary of peak calcium transients measured in
616 the shaded windows in K on correct and reward omission lever trials (n=81 dendrites, 3 animals,
617 3 sessions). N) Mean timecourses of calcium transients averaged across all dendrites for correct
618 (black) and reward omission (dark blue) trials. Vertical bars represent the lick rate averaged
619 across trials for all reward omission sessions.
620
621 **Supplemental Figures**
622 **Figure 1.** Mapping of motor output driven by Arch and electrical stimulation of superficial
623 cerebellar cortex. A) Schematics of the results of Arch stimulation over a grid of sites in lobule
624 simplex (Sim) and Crus I for all five mice. Colors denote outcome of stimulation. B) Same as A
625 for three mice tested with electrical microstimulation.
626
627 **Figure 2**. Retention and extinguishment of learning for cue prediction regime. A) Average
628 reaction times relative to cue for the first (left) and second (right) sessions where animals
629 performed 0.5 s cue prediction on consecutive training days (n=17 sessions, 5 mice). Error bars
630 are ±SEM across sessions. B) Same as A for 2 s cue prediction sessions (n=10 sessions, 6
631 mice). C) *Left,* example cumulative distributions of reaction times for cue reaction sessions
632 immediately surrounding a cue prediction session (session 0). Trials from the cue prediction
633 session include only the last 1/3 of the session when the animal was anticipating the cue timing.
634 *Right,* summary of distribution skewness across cue reaction sessions immediately surrounding
635 cue prediction sessions. D) Same as A for pairs of 0.5 s prediction sessions separated by 3 or
636 more cue reaction sessions (n=20 sessions, 10 mice).
637
638 **Figure 3**. Performance on cue prediction task in control and NBQX sessions. A-E) Summary
639 across experiments of average percent correct lever releases, baseline reaction time from the
640 visual cue, mean reaction time variance, mean duration to press, number of trials performed, and
641 the duration of behavioral sessions. n=44 0.5 s, n=9 1.0 s, n=6 1.5 s, n=30 2.0 s, n=26 Δt, n=14
642 0.5 s NBQX. For each cue delay, the minimum and maximum (x,y) number of trials performed in
643 single sessions was: 0.5 s: (309, 700) 1 s: (252, 900) 1.5 s: (202, 775) 2 s: (278,1185) Δt: (313,
644 772) 0.5 s NBQX: (227, 429). F_i) Individual (top) and average (bottom) lever trajectories aligned

645 to lever press (left) and release(right) segregated by duration into quartiles for a representative
646 0.5 s cue prediction session. F_{ii}) Same as F_i for a representative 0.5 s cue prediction session in
647 NBQX. G) Summary of press (left) and release (right) quartiles across experiments for control
648 (top; n=15 sessions) and NBQX (bottom; n=14 sessions) experiments. H) Summary of the ratio
649 between press and release ranges (difference between 1st and 4th quartile) for control (black) and
650 NBQX (blue) experiments.
651
652 **Figure 4.** Pharmacological modulation of complex spiking in lobule simplex. A) Single unit
653 recordings during NBQX application to LS. Top, summary of complex spike rates in control and
654 after application of NBQX for individual cells (black; n=9 cells, 5 mice) and the average of all cells
655 (red). Error bars are ±SEM across cells. Bottom, same as top for simple spike rates. Note that
656 NBQX strongly reduces complex but not simple spike rates. B) (top) Raw epifluorescence images
657 from parasagittal cerebellar sections showing fluorescein labeling after surface application to
658 lobule simplex *in vivo* (methods, 3 mice). (bottom) Pixel masks from the same images above.
659 Pixels were thresholded at 30% of maximum value to visualize and quantify fluorescein labeling.
660 C) Summary of mediolateral fluorescein spread across sections. (n=3 animals).
661
662 **Figure 5**. Segmentation of PC dendrites from imaging experiments. A) Example single photon
663 imaging field of view (left) is segmented to mask individual dendrites (right) used for subsequent
664 single cell analysis. Scale bar = 100 μm. B) Example timecourse of raw fluorescence (top) from
665 the circled dendrite in A showing individual calcium transients identified (gray circles) according
666 to peaks in the first derivative of the fluorescence trace (bottom). C) Same as A for an example
667 two photon field of view. Note that while PC somata are visible (round, top right), image
668 segmentation does not extract activity from these structures. Scale bar = 100 μm. D) Same as B
669 for the experiment in C. E) Top, example time course of a single unit PC recording from an
670 awake mouse illustrating detection of complex spikes (gray circles). Bottom, overlay of individual
671 simple (left) and complex (right) spike waveforms (gray) and the average waveform (black). F)
672 Summary of spike rates across all two photon dendrite imaging sessions (blue; n=1051 dendrites)
673 and acute single unit recordings (n=11 units).
674
675 **Figure 6**. Single unit PC recordings of complex spiking during the cue prediction task. A)
676 Schematic of the trial structure schematic, where a constant cue delay of 500ms was imposed on
677 each trial. B) Mean normalized complex spike rate (methods) from single unit recordings (40 PCs,
678 8 mice) aligned to lever release for correct (black) and early (red) trials during the cue prediction
679 task.
680

681 **Figure 7.** Differential complex spiking on correct and early release trials is not driven by motor
682 signals due to licking. A) Example imaging data from an inter-trial interval (ITI) showing a lick
683 responsive cell (top, dark blue) and a lick unresponsive cell (bottom, black) in the same field of
684 view. B) Averaged lick triggered calcium transients for the lick responsive cell (dark blue) and a
685 lick unresponsive cell (black) in A). C) Mean lick triggered calcium transient across all lick
686 responsive (dark blue) and lick unresponsive (black) cells. D) Summary of the Spearman's
687 correlation between lick rate and amplitude of the calcium transient in each frame across trials for
688 lick responsive (dark blue) and lick unresponsive cells (grey). Red points indicate the mean ±
689 SEM across dendrites (447 dendrites, 6 animals and 10 sessions) E) Mean lick triggered calcium
690 transients for lick responsive neurons only in response to either a single lick (dark blue) or a lick
691 bout (3 or more licks with ≤ 300 ms between licks, blue). F) Mean lever release-evoked calcium
692 transients across neurons for correct (black) and early (red) lever releases for lick unresponsive
693 neurons only. G) Summary comparing the amplitude of calcium transients on correct and early
694 lever releases for lick unresponsive cells only.
695
696 **Figure 8.** Example single trial and session average calcium transients from 2-photon imaging. A)
697 Example single trial data from an individual dendrite showing the normalized calcium transient
698 across an early release trial from before lever press to after the lever release. B) Same as A) but
699 for a correct trial, including the time of cue presentation. C) Mean calcium transients across trials
700 for the dendrite in A and B. D) Single trial example, aligned to lever release, showing all neurons
701 from the experiment illustrated in Fig. 5C on a correct trial over 1 second surrounding release.
702 Lever press is off scale. E) Same as D, but for an early release trial from the same imaging
703 session.
704
705 **Figure 9**. Mice have full control over the lever trajectory. A) Individual (top) and average (bottom)
706 lever trajectories aligned to lever press (left) and release (right) for manual lever depression
707 followed by unperturbed gravity return. B) Summary of press (left) and release (right) quartiles
708 across experiments for manual lever experiments (n=4). Note the lack of variability across
709 quartiles. C) Summary scatterplot comparing 20-80% rise times of lever press and release for
710 experiments where the lever was controlled by mice (black) and manual press (green) D)
711 Summary comparison measuring the difference from the mean of the slowest release quartile and
712 the fastest release quartile for experiments where the lever was controlled by mice (black) and
713 manual press (green). Lever trajectories were sorted according to duration in a window from
714 200ms before threshold crossing to the time of a threshold crossing half way between the top and
715 bottom of the total lever displacement. The slowest and fastest 25 trials were extracted for
716 comparison, and their average rise time was normalized by subtracting that of the mean trajectory

717 of the whole session. These results show that mice produce movements both slower and faster
718 than the mean, indicating full control over the lever trajectory.
719
720 **Methods:**
721 Mice
722 All experimental procedures using animals were carried out with the approval of the Duke
723 University Animal Care and Use Committee. All experiments were performed during light cycle
724 using adult mice (>p60) of both sexes, randomly selected from breeding litters. All mice were
725 housed in a vivarium with normal light/dark cycles in cages with 1-5 mice. Imaging experiments
726 were performed using Tg(PCP2-Cre)3555Jdhu mice (Jackson Labs, 010536; n=12). Optogenetic
727 mapping experiments were conducted in PCP2-Cre animals crossed with Ai35(RCL-Arch/GFP)
728 (Jax 012735; n=5 mice). Single unit recording during the cue prediction task was performed in
729 wild type C57BL/6J mice (n= 8 mice). Additional behavioral experiments where imaging was not
730 performed were conducted in wild type C57BL/6J mice (n=18). We used two exclusion criteria for
731 animals in this study: (1) poor recovery or other health concerns following surgical intervention or
732 (2) missed virus injection, as determined by *in vivo* imaging and post-hoc histological analysis.
733
734 Surgical Procedures
735 3-10 hours prior to surgery, animals received dexamethasone (3mg/kg) and ketoprofen (5mg/kg).
736 Surgical procedures were performed under anesthesia, using an initial dose of ketamine/xylazine
737 (50mg/kg and 5mg/kg) 5 minutes prior to surgery and sustained during surgery with 1.0-2.0%
738 isoflurane. Toe pinches and breathing were used to monitor anesthesia levels throughout
739 surgeries. Body temperature was maintained using a heating pad (TC-1000 CWE Inc.). Custom-
740 made titanium headplates (HE Parmer) were secured to the skull using Metabond (Parkell). For
741 imaging experiments, a 3mm diameter craniotomy was made over the lobule simplex
742 approximately 1.4mm lateral and 2.8mm posterior to lambda, and glass cover slips consisting of
743 two 3mm bonded to a 5mm coverslip (Warner Instruments No. 1) with index matched adhesive
744 (Norland No. 1) were secured in the craniotomy using Metabond. Buprenex (0.05mg/kg) and
745 cefazolin (50mg/kg) were administered following surgery twice a day for two days. Following a
746 minimum of 4 recovery days, animals were water deprived for 3 days, or until body weight
747 stabilized at 85% of initial weight, and were habituated to head restraint (3-5 days) prior to
748 behavioral training.
749 For imaging experiments, the glass cover slip was removed following behavioral training,
750 and mice were injected (WPI UMP3) with AAV1.CAG.Flex.GCaMP6f.WPRE.SV40 (UPenn vector
751 core, titer = 9.40×10^{12} or 7.60×10^{12}). 150 nL virus diluted 1:1-1:5 in ACSF was injected at a rate of

752 30nl/min and a depth of 150 μm at 1-3 sites in dorsal lobule simplex. Imaging was performed
753 beginning 14 days following injection.
754 For *in vivo* pharmacology experiments, a 3mm craniotomy was performed over lobule
755 simplex of headposted mice, and the dura mater was peeled back at the center of the craniotomy.
756 10uL of combined NBQX (300 μM) and CPP (30 μM) was applied into a well surrounding the
757 craniotomy on the surface of the cerebellum 20 minutes prior to behavioral training. In 8 of 14
758 experiments, MCPG (30 μM) was also included to block metabotropic glutamate receptors.
759 Because there no significant differences in performance across these two groups, all data were
760 pooled for analysis. During behavior, a second drug application of 10uL was administered 20 and
761 40 minutes into the task, and depending on the duration of training, a third dose was applied after
762 1 hour. Craniotomies were subsequently covered with silicone elastomer (WPI, Inc.) prior to
763 returning animals to their home cage. To quantify the spread of pharmacological agents in the
764 cerebellum, 10 μL of fluorescein dye (Sigma-Aldrich #F6377, 1mM in aCSF) was applied to the
765 craniotomy in 3 animals with the same method and timecourse as for drug applications. Following
766 standard histological processing and imaging (below), labeling was quantified by creating a binary
767 pixel mask thresholded at 30% of the maximum fluorescence value for each experiment. Dye
768 labeling was then measured using the area of these pixel masks (Supp. Fig. 4 B,C).
769
770 Behavior
771 During behavioral training, animals were head-fixed and placed in front of a computer monitor,
772 lever and reward delivery tube. Animals were trained to self-initiate trials by depressing the lever
773 using their right forepaw, and required to successfully hold the lever in the down position for
774 randomized intervals ranging between 500ms and 5 s on the cue reaction paradigm before
775 performing the cue prediction paradigm. For both paradigms, a high contrast hold cue was present
776 at all times, including the intertrial interval (ITI), and transitioned 90 degrees to the release cue on
777 each trial at the instructed time of release until the animal either released the lever or 1 second
778 had passed. Lever releases within one second of the release cue were rewarded immediately at
779 the time of lever release (0.01 M saccharine). Immediately following any lever release, a solenoid
780 was engaged to prevent lever press during the ITI. Following the ITI (3-6 s), the solenoid is
781 lowered, allowing the mouse to self initiate a new trial. During training, a 1-3 second 'timeout'
782 was implement to punish early lever releases. No timeouts were used in fully trained animals for
783 imaging or behavior data collection sessions. For reward omission sessions, 20% of randomly
784 determined correct lever releases were unrewarded. Animals used for imaging experiments
785 performed the cue reaction task with a mean peak percent correct of 79.7 ± 0.23% achieved in
786 26 ± 2 training days. On imaging days animals performed a range of 150 to 580 trials per session
787 with a mean of 273.9 ±13.1 trials. Behavioral parameters including lever press, lever release and

788 licking were monitored using Mworks (http://mworks-project.org) and custom software written in
789 MATLAB (Mathworks). To assess the degree of lever control by the mice, the dynamics of lever
790 press and release trajectories were compared to lever presses initiated by the experimenter
791 where the lever was allowed to return to the rest position on its own (Supp. Fig. 9). These results
792 demonstrate that mice moved the lever both faster and slower than its intrinsic kinematics, and
793 thus had full control over its trajectory. Licking was measured with electrical contact circuit. Inter-
794 trial intervals ranged from 3 to 5 seconds.
795
796 Calcium Imaging
797 *Wide-field imaging*: Single photon imaging was performed using a customized microscope (Sutter
798 SOM) affixed with a 5x objective (Mitutoyo, 0.14NA) and CMOS camera (Qimaging, Rolera em-
799 c^2). Excitation (470 nm) was provided by an LED (ThorLabs, M470L3), and data were collected
800 through a green filter (520-536 nm band pass, Edmund Optics) at a frame rate of 10Hz, with a
801 field of view of 3.5x3.5mm at 1002x1004 pixels.
802
803 *Two-Photon Imaging*: Two-photon imaging was performed with a resonant scanning microscope
804 (Neurolabware) using a 16x water immersion objective (Nikon CFI75 LWD 16xW 0.80NA).
805 Imaging was performed using a polymer to stabilize the immersion solution (MakingCosmetics,
806 0.4% Carbomer 940). A Ti:Sapphire laser tuned to 920nm (Spectra Physics, Mai Tai eHP
807 DeepSee) was raster scanned via a resonant galvanometer (8 kHz, Cambridge Technology) onto
808 the brain at a frame rate of either 30 Hz with a field of view of either 1030 μm x 581 μm (796 x
809 264 pixels) or 555 μm x 233 μm (796 x 264 pixels), or 15.5Hz with a field of view of 555 μm x 452
810 μm and (796 x 512 pixels). Data were collected through a green filter (510 ± 42 nm band filter
811 (Semrock)) onto GaAsP photomultipliers (H10770B-40, Hamamatsu) using Scanbox software
812 (Neurolabware). A total of 12 mice were used for imaging experiments (10 mice for wide-field, 11
813 mice for two-photon, 12 mice total).
814
815 Single Unit Recordings and Optogenetics
816 Acute single unit recordings were performed in awake animals by performing a craniotomy over
817 lobule simplex and inserting a multi-electrode silicone probe (Neuronexus, A4x8-5mm-100-400-
818 177-A32, 4 shanks, 8 site/shank at 100 μm spacing) using a Cerebus multichannel acquisition
819 system (Blackrock Microsystems, Salt Lake City). For single unit recordings obtained in the cue
820 prediction task (Supp. Fig. 6), chronically implanted electrode arrays were used (Dual drive
821 movable electrode bundles with 8 tungsten electrodes (23 μm) in each cannula or 16 tungsten
822 electrodes bundle in one cannula, Innovative Neurophysioloy Inc). Electrode arrays were
823 implanted using stereotaxic coordinates to target lobule simplex at AP 6.2; ML 2.0. Electrode

824 bundles were inserted into lobule simplex at a depth of approximately 0.2-0.3 mm. The implant
825 was encased in Metabond for stability.
826 For both recording conditions, continuous recording data was bandpass filtered with a 2-
827 pole Butterworth between 250 Hz and 5 kHz and referenced against an electrode with no spikes
828 using Spike2. Single units were isolated by amplitude thresholding. Template waveforms were
829 defined and characterized by their width and peak, and PCA of waveforms was done in off-line in
830 Spike2.
831 Complex spikes and simple spikes were discriminated as in de Solages et al.[61], first on
832 the basis of their stereotypical waveform. Complex spikes typically had a multi-wavelet form,
833 including a large positive peak within 6ms following spike initiation. Manual identification of 10-
834 20 complex spikes was used to generate a mean template waveform, which was then compared
835 to all other spikes for a given unit using the Spearman rank order correlation coefficient. The
836 combination of Spearman coefficients and the magnitude of the positive waveform deflection was
837 used to segregate complex and simple spikes. The presence of a post-complex spike pause (20
838 ms or more) in simple spike firing was verified by cross-correlogram for all isolated single units.
839 Complex spike rates for the cue prediction task were normalized to the baseline firing rate
840 determined in a one-second window during the ITI according to: (FR-baseline)/baseline) (Supp.
841 Fig. 6).
842 For optogenetic mapping of the dorsal cerebellum, an optical fiber (0.39 NA, 400 µm core
843 multimode, ThorLabs FT400EMT) coupled to a 532 nm laser (Optoengine, MGL-III-532) was
844 positioned above the cranial window using a micromanipulator (Scientifica PatchStar).
845
846 Histology
847 Mice were deeply anesthetized with ketamine/xylazine (200mg/kg & 30mg/kg respectively, IP)
848 then perfused with PBS then 4% paraformaldehyde. 100um sagittal sections were cut using a
849 vibratome (Pelco 102). Cerebellar slices were then mounted using a mounting medium (Southern
850 Biotech Fluoromount-G or DAPI Fluoromount-G) and imaged with a fluorescence microscope
851 (Nikon Eclipse 80i).
852
853 Data Analysis
854 *Behavior:* Behavior sessions were only analyzed within the time range of active task
855 performance. Accordingly, the last trial of each session was determined by the occurrence of
856 either two consecutive failed trials (in which the mouse did not release the lever in response to
857 the cue) or two consecutive trials with post-ITI duration to press longer than 1.5x the session
858 average.

Reaction times were measured using lever releases within the reward window as well as those occurring 200ms prior to the reward cue to account for predictive responses. Reaction times are plotted as a binned average of five trials. Initial reaction times were calculated according to the y-intercept of the linear regression of the first fifty trials. Final reaction time at the end of each session was calculated by averaging the reaction times of trials 200-250.

The symmetry of reaction time data about the sample mean was measured to test the extinguishment of learning after following cue prediction sessions according to skewness. Sample skewness was defined by

$$s = \frac{E(\mu - X)^3}{\sigma^3}$$

where μ is the mean of X, $E(*)$ is the expected value of the quantity $*$, and σ is the standard deviation of X. Thus, for a given sample x, this calculates:

$$\frac{\frac{1}{n}\sum_{i=1}^{n}(x_i - \bar{x})^3}{\left(\sqrt{\frac{1}{n}\sum_{i=1}^{n}(x_i - \bar{x})^2}\right)^3}$$

for $x_i \in x$, where $\bar{x}$ is the sample mean.

Movement trajectories were measured using a lever affixed to a rotary encoder (US Digital) with a 60mm radius and 1250 pulses per revolution. Encoder values were collected at 1000 Hz, and trajectories were calculated by up-sampling at 200 μs (5000 Hz) using nearest-neighbor interpolation. Pulse number was converted to degrees, and the vertical displacement in millimeters was calculated using the chord length of the leaver displacement angle. 20-80% rise times were calculated using normalized average trajectories. Presses and releases were sorted according to duration in a window from 200ms before threshold crossing to the time of a threshold crossing half way between the top and bottom of the total lever displacement.

Wide-field imaging: Imaging analysis were performed using custom MATLAB code. Regions of interest (ROIs) were selected within empirically defined forelimb movement region of lobule simplex according to the spread of GCaMP expression. Window location and the lobule identity were identified according to folia patterns visible through the cranial window, landmarks recorded during surgery, and post-hoc histology. Baseline fluorescence (F) was measured on a trial-by-trial basis during the inter-trial interval (ITI) as the mean fluorescence 900 to 200ms before trial initiation. Normalized fluorescence (ΔF/F) was calculated according to the cumulative activity within an ROI, or on a pixel by pixel basis. Lever hold times <200ms in total, or > 1 s after the

visual cue were exceedingly rare, and thus excluded from analysis. Lever releases between 200ms and 1000ms following the visual cue were classified as correct, and releases prior to visual cue were classified as early. Lever releases ≤200 ms following the visual cue were considered too fast to be reactions to the cue based on average reaction time distributions. Peak ΔF/F was measured on a trial by trial basis in the time window from 100ms before to 400 ms after lever release. Note that differences in the timing of single trial calcium transient peaks produce smaller amplitudes for ΔF/F timecourses as compared to reported peak ΔF/F measurements. Spearman's correlation between lick rate and peak ΔF/F within sessions was calculated according to the lick rate within 500 ms following each lever release and the peak calcium transient for each trial. For this correlation analysis, trials without licking were removed, and only sessions with 7 or more trials in each condition were included.

Meta K-means analysis and Cluster Correlations: Images were first registered to reduce motion artifacts, and then thresholded at 70% of maximum intensity for each frame to remove background noise. Images were downsampled 5-fold in both X and Y. Baseline F was defined as the averaged fluorescence across the entire movie for each pixel, and used to normalize change in fluorescence (ΔF/F). ΔF/F was then re-normalized to the maximum ΔF/F during the entire movie for each pixel. The repeated k-means clustering algorithm (meta-k-means) separated pixels to cluster centroids based on a pairwise correlation distance function using Pearson's linear correlation coefficient (r). The final clusters were determined by first thresholding all the k-means results at 800 out of 1000 runs, and then by merging highly correlated clusters based on Dunn's index. Clusters occupying less than 3% of the total imaging field were excluded from further analysis. Intra-cluster and inter-cluster correlation coefficients were calculated between 100 ms before and 300 ms after lever release for both correct and early trials on a frame by frame basis. To test for differences in the relationship between spike rates and correlation coefficients between trial types, paired clusters from each distribution were resampled with replacement and fit with a line to measure the y-intercept 1000 times. Statistical significance was computed according to the 95% confidence interval of the distribution of y-intercept difference values (difference between y-intercepts 0.0375 ± 0.0013, 95% confidence interval [0.0349, 0.0402]).

Two-photon imaging: Motion in the XY plane was corrected by sub-pixel image registration. To isolate signals from individual PC dendrites, we utilized principal component analysis (PCA) followed by independent component analysis (ICA). Final dendrite segmentation was achieved by thresholding the smoothed spatial filters from ICA. A binary mask was created by combining highly correlated pixels (correlation coefficient > 0.8) and removing any overlapped regions between segmented dendrites. Notably, image segmentation using these criteria did not extract

928 PC soma, which were clearly visible in many single- and two-photon imaging experiments.
929 Fluorescence changes (ΔF) were normalized to a window of baseline fluorescence (F) between
930 500ms and 100ms preceding trial initiation. Responses were categorized as significant ($p<0.05$)
931 according to a one-tailed t-test if the $\Delta F/F$ in a 200 ms window surrounding lever press or release
932 was larger than that from a 500 ms window immediately preceding lever movement. To extract
933 events on single trials used for estimation of complex spike rates and event amplitudes, the first
934 derivative of the raw fluorescence trace was thresholded at 2.5 standard deviations from baseline.
935 The same methods were used to extract events for the subset of single photon experiments
936 described in Supp. Fig. 5. For single trial amplitude measurements, only events well separated
937 in time (greater than 650ms from the next event) were considered; however, for measurements
938 of rates, all events separated by at least one frame were included. Note that rate estimates are
939 thus likely to be lower than actual rates, particularly for single photon imaging where data were
940 collected at 100 ms intervals. Peak calcium transients on reward omission trials and on early
941 release trials were quantified in two time windows (Fig. 8). Window 1 spanned the first 100 ms
942 after lever release, and window 2 spanned 175 ms that began 165ms after lever release.
943 Spearman's correlation was calculated between lick rate and the peak calcium transient within
944 sessions on a frame by frame basis for each trial in a window spanning 500 ms after lever release.
945 Correlation values for correct and early release trials for each cell were averaged separately.
946 Some neurons showed responses to licking, as defined by a mean lick-triggered calcium transient
947 that was significantly larger ($p<0.05$) with respect to baseline (Supp. Fig. 7). Lick triggered
948 averages were constructed from licks presumed to be spontaneous that occurred during the inter-
949 trial interval (Supp. Fig. 7).
950
951 *Additional statistics and data sharing*: Data are presented as mean ± S.E.M., unless stated
952 otherwise. Statistical tests were two-sided, and analyses of variance (ANOVA) were performed
953 when more than two groups were tested. Differences were considered statistically significant
954 when $P < 0.05$. No correction for multiple comparisons was applied. No statistical methods were
955 used to predetermine sample sizes. Data collection and analysis were not performed blind to the
956 conditions of the experiments, but data collection relied on automatized measurements and
957 subsequent analysis was based on code uniformly applied across experimental conditions. Data
958 analysis code are available on GitHub (access available upon request). The data that support the
959 findings of this study are available from the corresponding author upon reasonable request.
960
961
962 **References**
963

964 1. Albus, J.S. A theory of cerebellar function. *Mathematical Biosciences* **10**, 25-61 (1971).
965 2. Ito, M. Neural design of the cerebellar motor control system. *Brain Res* **40**, 81-84 (1972).
966 3. Marr, D. A theory of cerebellar cortex. *J Physiol* **202**, 437-470 (1969).
967 4. Ito, M., Sakurai, M. & Tongroach, P. Climbing fibre induced depression of both mossy fibre
968 responsiveness and glutamate sensitivity of cerebellar Purkinje cells. *J Physiol* **324**, 113-134
969 (1982).
970 5. Ekerot, C.F. & Kano, M. Long-term depression of parallel fibre synapses following
971 stimulation of climbing fibres. *Brain Res* **342**, 357-360 (1985).
972 6. Sakurai, M. Synaptic modification of parallel fibre-Purkinje cell transmission in in vitro
973 guinea-pig cerebellar slices. *J Physiol* **394**, 463-480 (1987).
974 7. Miyakawa, H., Lev-Ram, V., Lasser-Ross, N. & Ross, W.N. Calcium transients evoked by
975 climbing fiber and parallel fiber synaptic inputs in guinea pig cerebellar Purkinje neurons. *J*
976 *Neurophysiol* **68**, 1178-1189 (1992).
977 8. Tank, D.W., Sugimori, M., Connor, J.A. & Llinas, R.R. Spatially resolved calcium dynamics
978 of mammalian Purkinje cells in cerebellar slice. *Science* **242**, 773-777 (1988).
979 9. Konnerth, A., Dreessen, J. & Augustine, G.J. Brief dendritic calcium signals initiate long-
980 lasting synaptic depression in cerebellar Purkinje cells. *Proc Natl Acad Sci U S A* **89**, 7051-7055
981 (1992).
982 10. Llinas, R. & Sugimori, M. electrophysiological properties of in vitro purkinje cell somata in
983 mammalian cerebellar slices. *J. Physiol.*, 171-195 (1980).
984 11. Eccles, J.C., Llinas, R. & Sasaki, K. The excitatory synaptic action of climbing fibres on the
985 Purkinje cells of the cerebellum. *J Physiol* **182**, 268-296 (1966).
986 12. Medina, J.F., Nores, W.L., Ohyama, T. & Mauk, M.D. Mechanisms of cerebellar learning
987 suggested by eyelid conditioning. *Current opinion in neurobiology* **10**, 717-724 (2000).
988 13. Ohyama, T.N.W.M.M. & Mauk, M. What the cerebellum computes. *Trends in*
989 *Neurosciences* **26**, 222-227 (2003).
990 14. Raymond, J.L., Lisberger, S.G. & Mauk, M.D. The cerebellum: a neuronal learning
991 machine? *Science* **272**, 1126-1131 (1996).
992 15. Schultz, S.R., Kitamura, K., Post-Uiterweer, A., Krupic, J. & Hausser, M. Spatial pattern
993 coding of sensory information by climbing fiber-evoked calcium signals in networks of
994 neighboring cerebellar Purkinje cells. *J Neurosci* **29**, 8005-8015 (2009).

995 16. Tsutsumi, S., *et al.* Structure-function relationships between aldolase C/zebrin II
996 expression and complex spike synchrony in the cerebellum. *J Neurosci* **35**, 843-852 (2015).
997 17. Ozden, I., Dombeck, D.A., Hoogland, T.M., Tank, D.W. & Wang, S.S. Widespread state-
998 dependent shifts in cerebellar activity in locomoting mice. *PLoS One* **7**, e42650 (2012).
999 18. De Gruijl, J.R., Hoogland, T.M. & De Zeeuw, C.I. Behavioral correlates of complex spike
1000 synchrony in cerebellar microzones. *J Neurosci* **34**, 8937-8947 (2014).
1001 19. Tang, T., Suh, C.Y., Blenkinsop, T.A. & Lang, E.J. Synchrony is Key: Complex Spike Inhibition
1002 of the Deep Cerebellar Nuclei. *Cerebellum* **15**, 10-13 (2016).
1003 20. Lee, K.H., *et al.* Circuit mechanisms underlying motor memory formation in the
1004 cerebellum. *Neuron* **86**, 529-540 (2015).
1005 21. Histed, M.H., Carvalho, L.A. & Maunsell, J.H. Psychophysical measurement of contrast
1006 sensitivity in the behaving mouse. *J Neurophysiol* **107**, 758-765 (2012).
1007 22. Chettih, S.N., McDougle, S.D., Ruffolo, L.I. & Medina, J.F. Adaptive timing of motor output
1008 in the mouse: the role of movement oscillations in eyelid conditioning. *Front Integr Neurosci* **5**,
1009 72 (2011).
1010 23. Gaffield, M.A., Amat, S.B., Bito, H. & Christie, J.M. Chronic imaging of movement-related
1011 Purkinje cell calcium activity in awake behaving mice. *J Neurophysiol* **115**, 413-422 (2016).
1012 24. Mukamel, E.A., Nimmerjahn, A. & Schnitzer, M.J. Automated analysis of cellular signals
1013 from large-scale calcium imaging data. *Neuron* **63**, 747-760 (2009).
1014 25. Najafi, F., Giovannucci, A., Wang, S.S. & Medina, J.F. Coding of stimulus strength via analog
1015 calcium signals in Purkinje cell dendrites of awake mice. *Elife* **3**, e03663 (2014).
1016 26. Ozden, I., Lee, H.M., Sullivan, M.R. & Wang, S.S. Identification and clustering of event
1017 patterns from in vivo multiphoton optical recordings of neuronal ensembles. *J Neurophysiol* **100**,
1018 495-503 (2008).
1019 27. Ozden, I., Sullivan, M.R., Lee, H.M. & Wang, S.S. Reliable coding emerges from
1020 coactivation of climbing fibers in microbands of cerebellar Purkinje neurons. *J Neurosci* **29**,
1021 10463-10473 (2009).
1022 28. Najafi, F., Giovannucci, A., Wang, S.S. & Medina, J.F. Sensory-driven enhancement of
1023 calcium signals in individual Purkinje cell dendrites of awake mice. *Cell Rep* **6**, 792-798 (2014).
1024 29. Najafi, F. & Medina, J.F. Beyond "all-or-nothing" climbing fibers: graded representation of
1025 teaching signals in Purkinje cells. *Front Neural Circuits* **7**, 115 (2013).

1026 30. Yang, Y. & Lisberger, S.G. Purkinje-cell plasticity and cerebellar motor learning are graded
1027 by complex-spike duration. *Nature* **510**, 529-532 (2014).
1028 31. Rudolph, S., Overstreet-Wadiche, L. & Wadiche, J.I. Desynchronization of multivesicular
1029 release enhances Purkinje cell output. *Neuron* **70**, 991-1004 (2011).
1030 32. Maruta, J., Hensbroek, R.A. & Simpson, J.I. Intraburst and interburst signaling by climbing
1031 fibers. *J Neurosci* **27**, 11263-11270 (2007).
1032 33. Kitamura, K. & Hausser, M. Dendritic calcium signaling triggered by spontaneous and
1033 sensory-evoked climbing fiber input to cerebellar Purkinje cells in vivo. *J Neurosci* **31**, 10847-
1034 10858 (2011).
1035 34. Brenowitz, S.D. & Regehr, W.G. Associative short-term synaptic plasticity mediated by
1036 endocannabinoids. *Neuron* **45**, 419-431 (2005).
1037 35. Eilers, J., Augustine, G.J. & Konnerth, A. Subthreshold synaptic Ca2+ signalling in fine
1038 dendrites and spines of cerebellar Purkinje neurons. *Nature* **373**, 155-158 (1995).
1039 36. Hartell, N.A. Strong activation of parallel fibers produces localized calcium transients and
1040 a form of LTD that spreads to distant synapses. *Neuron* **16**, 601-610 (1996).
1041 37. Wang, S.S., Denk, W. & Hausser, M. Coincidence detection in single dendritic spines
1042 mediated by calcium release. *Nat Neurosci* **3**, 1266-1273 (2000).
1043 38. Andersson, G. & Oscarsson, O. Climbing fiber microzones in cerebellar vermis and their
1044 projection to different groups of cells in the lateral vestibular nucleus. *Exp Brain Res* **32**, 565-579
1045 (1978).
1046 39. Apps, R. & Garwicz, M. Anatomical and physiological foundations of cerebellar
1047 information processing. *Nat Rev Neurosci* **6**, 297-311 (2005).
1048 40. Ackerley, R., Pardoe, J. & Apps, R. A novel site of synaptic relay for climbing fibre pathways
1049 relaying signals from the motor cortex to the cerebellar cortical C1 zone. *J Physiol* **576**, 503-518
1050 (2006).
1051 41. Kitazawa, S., Kimura, T. & Yin, P.B. Cerebellar complex spikes encode both destinations
1052 and errors in arm movements. *Nature* **392**, 494-497 (1998).
1053 42. Sugihara, I. & Shinoda, Y. Molecular, topographic, and functional organization of the
1054 cerebellar cortex: a study with combined aldolase C and olivocerebellar labeling. *J Neurosci* **24**,
1055 8771-8785 (2004).

1056 43. Sugihara, I., Wu, H.S. & Shinoda, Y. The entire trajectories of single olivocerebellar axons
1057 in the cerebellar cortex and their contribution to Cerebellar compartmentalization. *J Neurosci* **21**,
1058 7715-7723 (2001).
1059 44. Voogd, J., Pardoe, J., Ruigrok, T.J. & Apps, R. The distribution of climbing and mossy fiber
1060 collateral branches from the copula pyramidis and the paramedian lobule: congruence of
1061 climbing fiber cortical zones and the pattern of zebrin banding within the rat cerebellum. *J*
1062 *Neurosci* **23**, 4645-4656 (2003).
1063 45. Ekerot, C.F., Garwicz, M. & Schouenborg, J. Topography and nociceptive receptive fields
1064 of climbing fibres projecting to the cerebellar anterior lobe in the cat. *J Physiol* **441**, 257-274
1065 (1991).
1066 46. Oberdick, J., Baader, S.L. & Schilling, K. From zebra stripes to postal zones: deciphering
1067 patterns of gene expression in the cerebellum. *Trends Neurosci* **21**, 383-390 (1998).
1068 47. Zhou, H*., et al.* Cerebellar modules operate at different frequencies. *Elife* **3**, e02536
1069 (2014).
1070 48. Paukert, M., Huang, Y.H., Tanaka, K., Rothstein, J.D. & Bergles, D.E. Zones of enhanced
1071 glutamate release from climbing fibers in the mammalian cerebellum. *J Neurosci* **30**, 7290-7299
1072 (2010).
1073 49. Blenkinsop, T.A. & Lang, E.J. Synaptic action of the olivocerebellar system on cerebellar
1074 nuclear spike activity. *J Neurosci* **31**, 14708-14720 (2011).
1075 50. Bengtsson, F., Ekerot, C.F. & Jorntell, H. In vivo analysis of inhibitory synaptic inputs and
1076 rebounds in deep cerebellar nuclear neurons. *PLoS One* **6**, e18822 (2011).
1077 51. Person, A.L. & Raman, I.M. Purkinje neuron synchrony elicits time-locked spiking in the
1078 cerebellar nuclei. *Nature* **481**, 502-505 (2012).
1079 52. McElvain, L.E., Bagnall, M.W., Sakatos, A. & du Lac, S. Bidirectional plasticity gated by
1080 hyperpolarization controls the gain of postsynaptic firing responses at central vestibular nerve
1081 synapses. *Neuron* **68**, 763-775 (2010).
1082 53. Pugh, J.R. & Raman, I.M. Potentiation of mossy fiber EPSCs in the cerebellar nuclei by
1083 NMDA receptor activation followed by postinhibitory rebound current. *Neuron* **51**, 113-123
1084 (2006).
1085 54. Miles, F.A. & Lisberger, S.G. Plasticity in the vestibulo-ocular reflex: a new hypothesis.
1086 *Annu Rev Neurosci* **4**, 273-299 (1981).

1087 55. Ohmae, S. & Medina, J.F. Climbing fibers encode a temporal-difference prediction error
1088 during cerebellar learning in mice. *Nat Neurosci* **18**, 1798-1803 (2015).
1089 56. Matias, S., Lottem, E., Dugue, G.P. & Mainen, Z.F. Activity patterns of serotonin neurons
1090 underlying cognitive flexibility. *Elife* **6** (2017).
1091 57. Belova, M.A., Paton, J.J., Morrison, S.E. & Salzman, C.D. Expectation modulates neural
1092 responses to pleasant and aversive stimuli in primate amygdala. *Neuron* **55**, 970-984 (2007).
1093 58. Hayden, B.Y., Heilbronner, S.R., Pearson, J.M. & Platt, M.L. Surprise signals in anterior
1094 cingulate cortex: neuronal encoding of unsigned reward prediction errors driving adjustment in
1095 behavior. *J Neurosci* **31**, 4178-4187 (2011).
1096 59. Pearce, J.M. & Hall, G. A model for Pavlovian learning: variations in the effectiveness of
1097 conditioned but not of unconditioned stimuli. *Psychol Rev* **87**, 532-552 (1980).
1098 60. Roesch, M.R., Esber, G.R., Li, J., Daw, N.D. & Schoenbaum, G. Surprise! Neural correlates
1099 of Pearce-Hall and Rescorla-Wagner coexist within the brain. *Eur J Neurosci* **35**, 1190-1200 (2012).
1100 61. de Solages, C.*, et al.* High-frequency organization and synchrony of activity in the purkinje
1101 cell layer of the cerebellum. *Neuron* **58**, 775-788 (2008).
1102

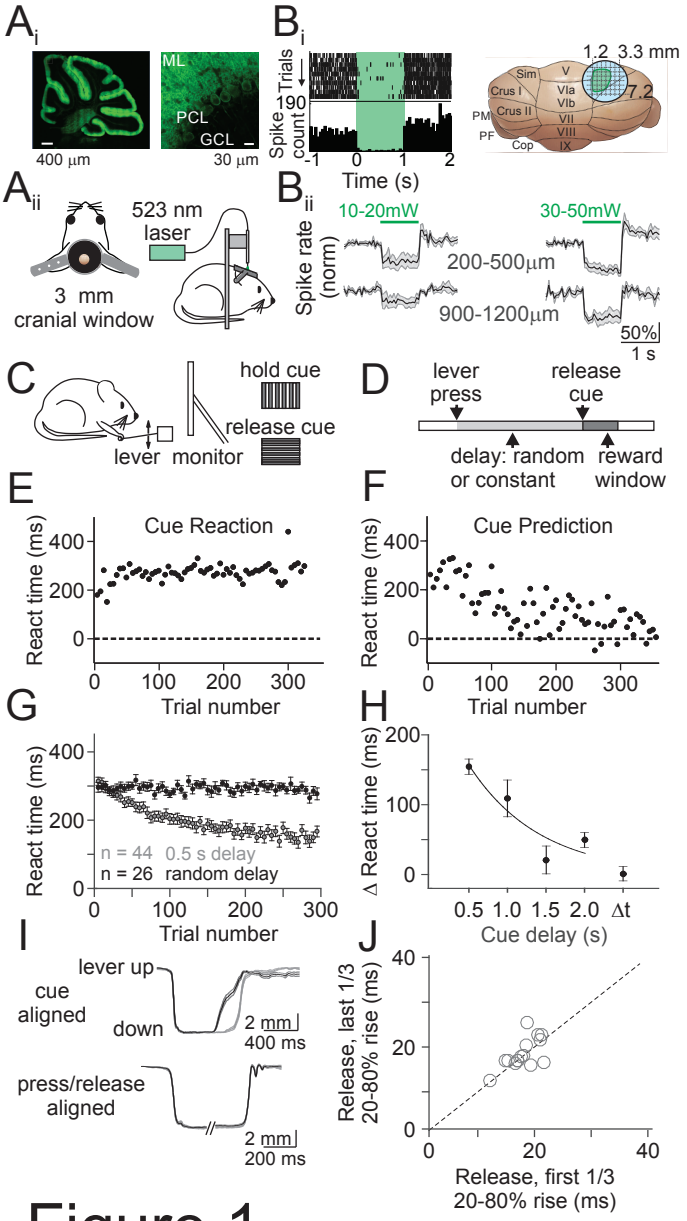
A_i
ML
PCL
GCL
400 µm
30 µm
B_i
Trials
190
Spike count
-1
0
1
2
Time (s)
1.2
3.3 mm
7.2
Sim
V
Crus I
VIa
VIb
Crus II
PM
VII
PF
VIII
Cop
IX
A_ii
523 nm laser
3 mm cranial window
B_ii
10-20mW
30-50mW
Spike rate (norm)
200-500µm
900-1200µm
50%
1 s
C
hold cue
release cue
lever
monitor
D
lever press
release cue
delay: random or constant
reward window
E
Cue Reaction
React time (ms)
400
200
0
0
100
200
300
Trial number
F
Cue Prediction
React time (ms)
400
200
0
0
100
200
300
Trial number
G
React time (ms)
400
200
0
n = 44 0.5 s delay
n = 26 random delay
0
100
200
300
Trial number
H
Δ React time (ms)
200
100
0
0.5
1.0
1.5
2.0
Δt
Cue delay (s)
I
lever up
cue aligned
down
2 mm
400 ms
press/release aligned
2 mm
200 ms
J
Release, last 1/3 20-80% rise (ms)
40
20
0
0
20
40
Release, first 1/3 20-80% rise (ms)

Figure 1

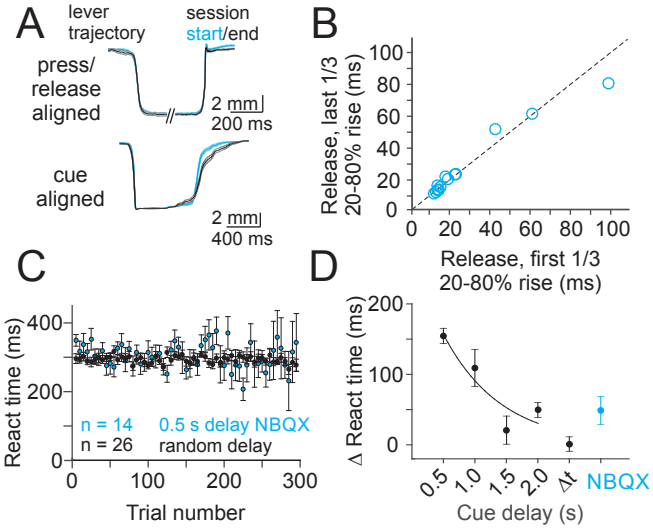
A
lever trajectory
session start/end
press/ release aligned
2 mm
200 ms
cue aligned
2 mm
400 ms
B
Release, last 1/3 20-80% rise (ms)
Release, first 1/3 20-80% rise (ms)
C
React time (ms)
n = 14
n = 26
0.5 s delay NBQX
random delay
Trial number
D
Δ React time (ms)
0.5
1.0
1.5
2.0
Δt
NBQX
Cue delay (s)

Figure 2

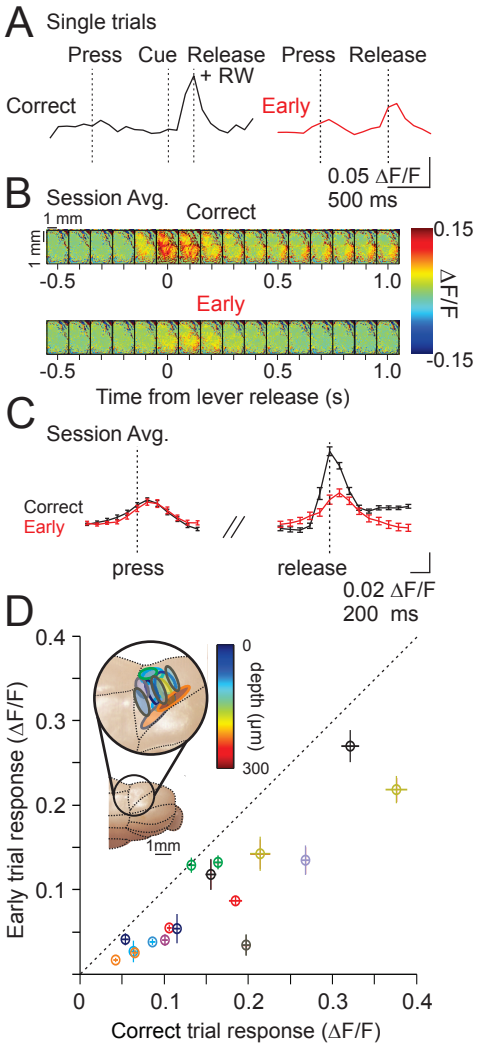
A
Single trials
Press
Cue
Release
+ RW
Press
Release
Correct
Early
0.05 ΔF/F
500 ms
B
Session Avg.
Correct
1 mm
1 mm
-0.5
0
0.5
1.0
Early
-0.5
0
0.5
1.0
0.15
ΔF/F
-0.15
Time from lever release (s)
C
Session Avg.
Correct
Early
press
release
0.02 ΔF/F
200 ms
D
0.4
0.3
0.2
0.1
Early trial response (ΔF/F)
0
0.1
0.2
0.3
0.4
Correct trial response (ΔF/F)
0
depth (μm)
300
1mm

Figure 3

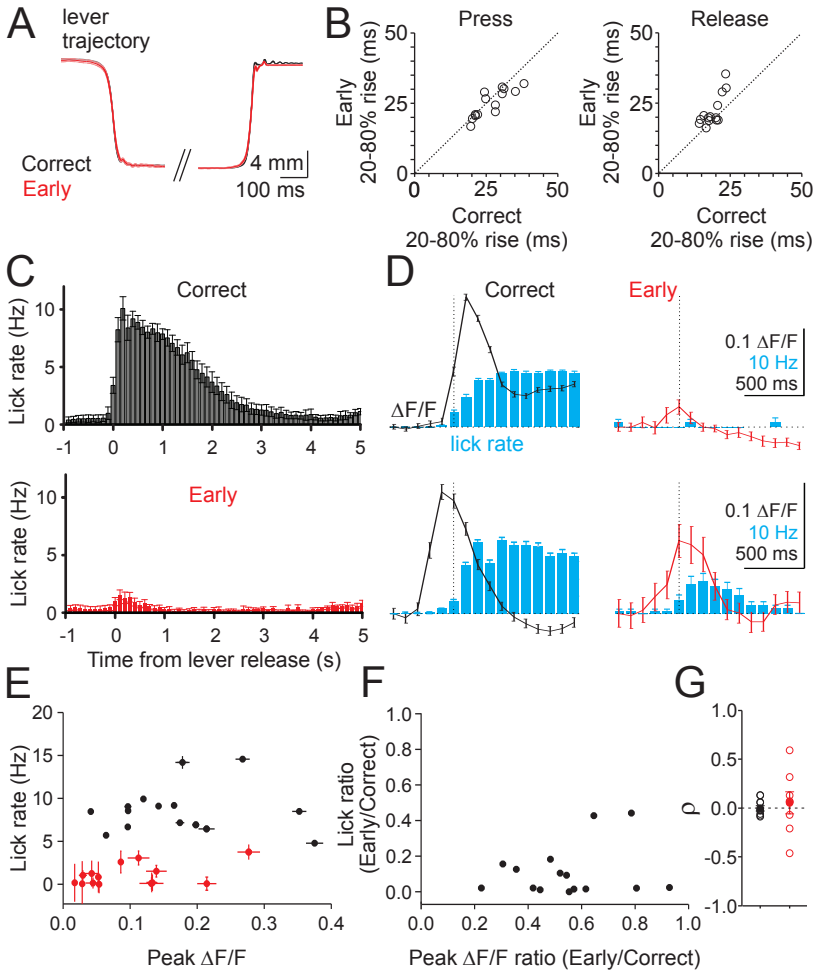
A
lever
trajectory
Correct
Early
4 mm
100 ms
B
Press
Release
Early
20-80% rise (ms)
Correct
20-80% rise (ms)
C
Correct
Early
Lick rate (Hz)
Time from lever release (s)
D
Correct
Early
ΔF/F
lick rate
0.1 ΔF/F
10 Hz
500 ms
E
Lick rate (Hz)
Peak ΔF/F
F
Lick ratio
(Early/Correct)
Peak ΔF/F ratio (Early/Correct)
G
ρ

Figure 4

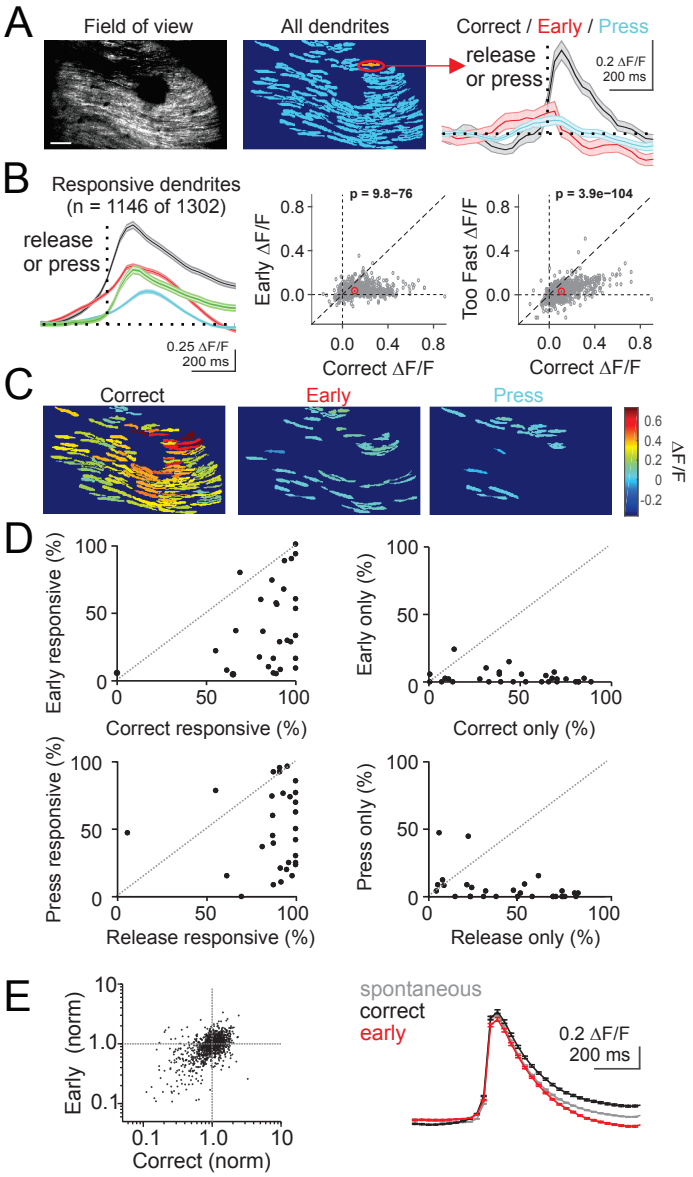
A
Field of view
All dendrites
Correct / Early / Press
release
or press
0.2 ΔF/F
200 ms
B
Responsive dendrites
(n = 1146 of 1302)
release
or press
0.25 ΔF/F
200 ms
p = 9.8−76
Early ΔF/F
Correct ΔF/F
p = 3.9e−104
Too Fast ΔF/F
Correct ΔF/F
C
Correct
Early
Press
ΔF/F
D
Early responsive (%)
Correct responsive (%)
Early only (%)
Correct only (%)
Press responsive (%)
Release responsive (%)
Press only (%)
Release only (%)
E
Early (norm)
Correct (norm)
spontaneous
correct
early
0.2 ΔF/F
200 ms

Figure 5

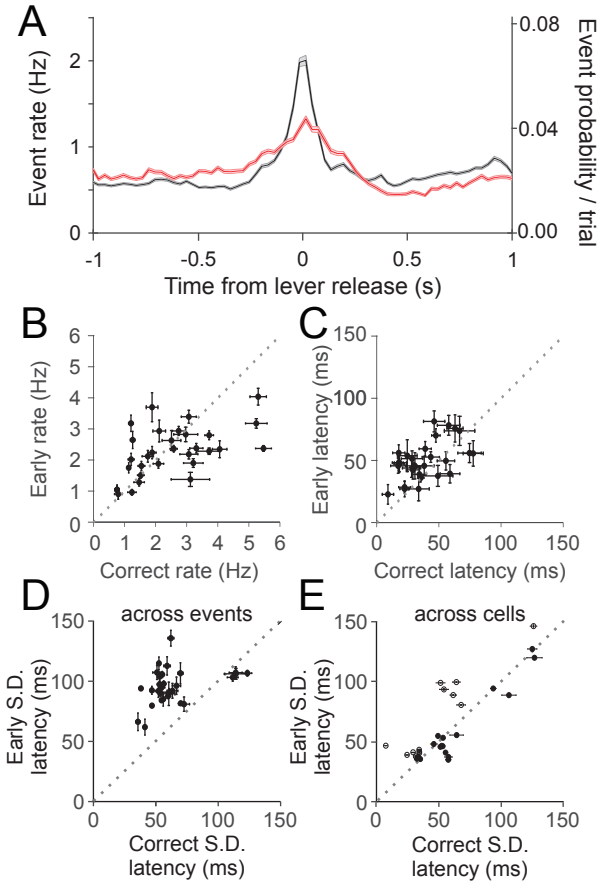
A
Event rate (Hz)
Event probability / trial
Time from lever release (s)
B
Early rate (Hz)
Correct rate (Hz)
C
Early latency (ms)
Correct latency (ms)
D
across events
Early S.D. latency (ms)
Correct S.D. latency (ms)
E
across cells
Early S.D. latency (ms)
Correct S.D. latency (ms)

Figure 6

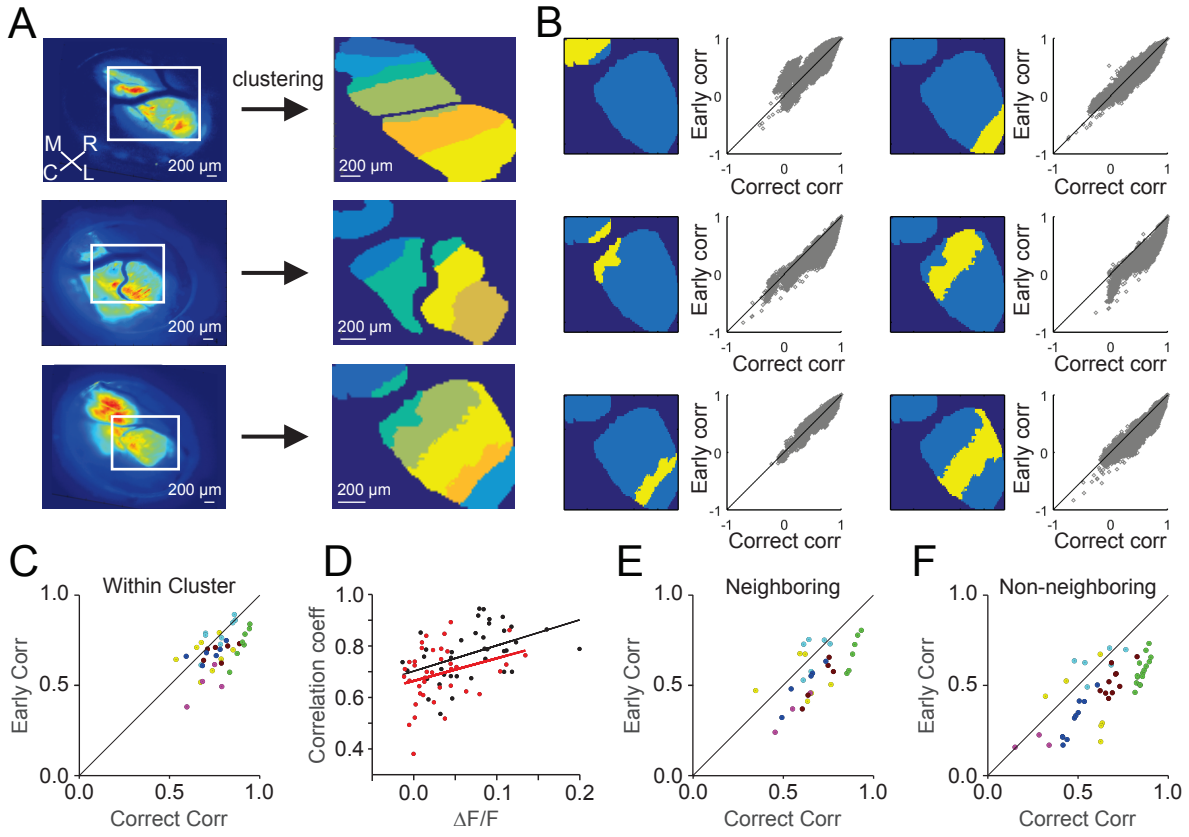
A
clustering
M
R
C
L
200 µm
B
Early corr
Correct corr
C
Within Cluster
Early Corr
Correct Corr
D
Correlation coeff
ΔF/F
E
Neighboring
F
Non-neighboring

Figure 7

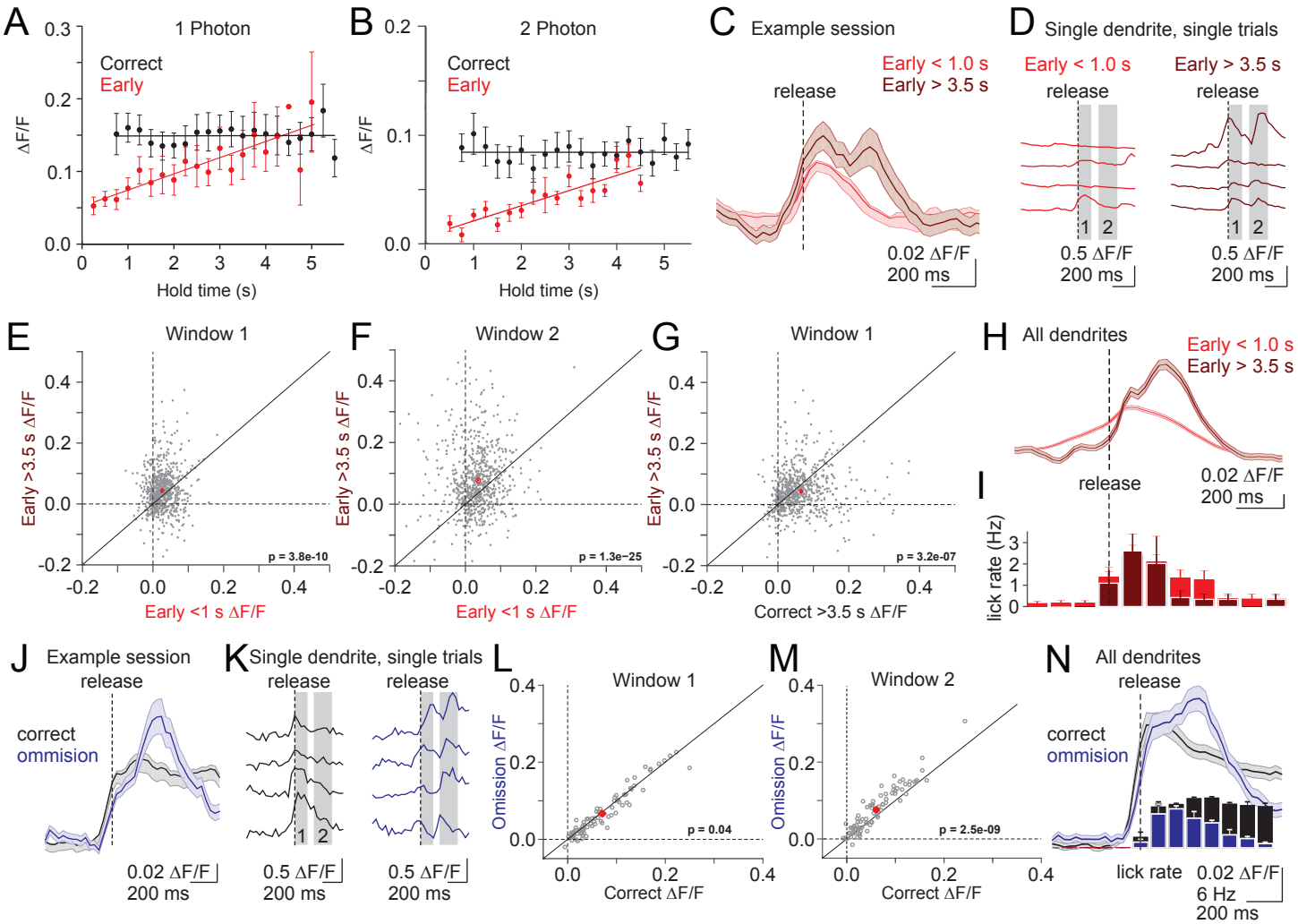
A
1 Photon
Correct
Early
ΔF/F
Hold time (s)
B
2 Photon
Correct
Early
ΔF/F
Hold time (s)
C
Example session
release
Early < 1.0 s
Early > 3.5 s
0.02 ΔF/F
200 ms
D
Single dendrite, single trials
Early < 1.0 s
Early > 3.5 s
release
1
2
0.5 ΔF/F
200 ms
E
Window 1
Early >3.5 s ΔF/F
Early <1 s ΔF/F
p = 3.8e-10
F
Window 2
Early >3.5 s ΔF/F
Early <1 s ΔF/F
p = 1.3e−25
G
Window 1
Early >3.5 s ΔF/F
Correct >3.5 s ΔF/F
p = 3.2e-07
H
All dendrites
Early < 1.0 s
Early > 3.5 s
release
0.02 ΔF/F
200 ms
I
lick rate (Hz)
J
Example session
release
correct
ommision
0.02 ΔF/F
200 ms
K
Single dendrite, single trials
release
1
2
0.5 ΔF/F
200 ms
L
Window 1
Omission ΔF/F
Correct ΔF/F
p = 0.04
M
Window 2
Omission ΔF/F
Correct ΔF/F
p = 2.5e-09
N
All dendrites
release
correct
ommision
lick rate
0.02 ΔF/F
6 Hz
200 ms

Figure 8

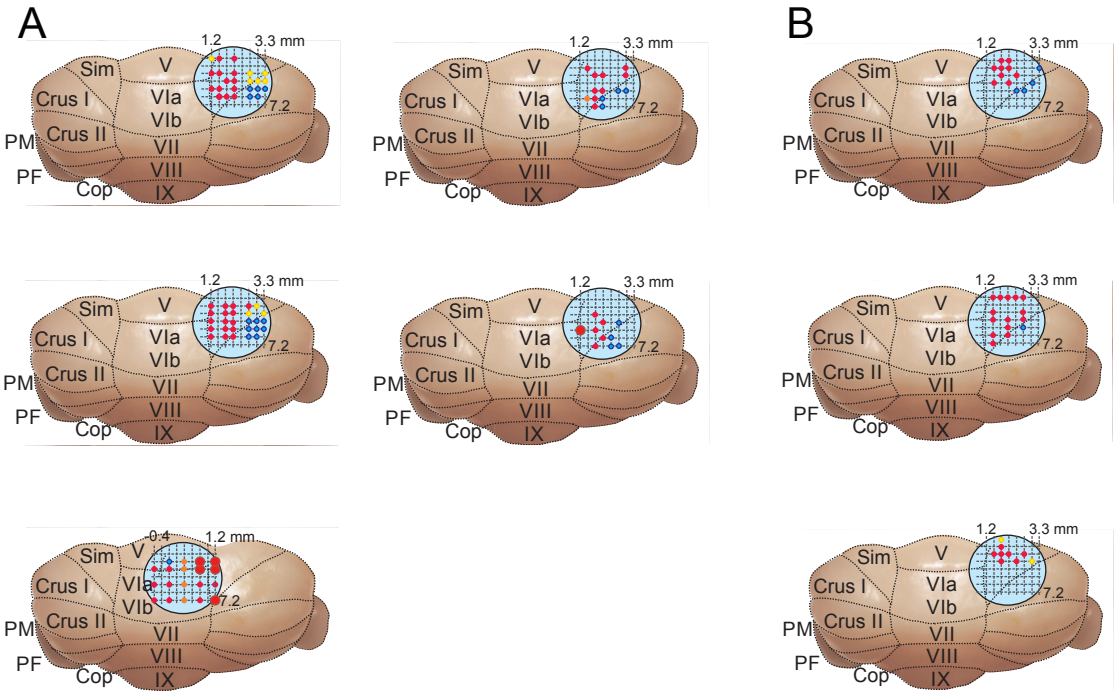

Arch: 5 mice
10-50mW, one Step pulse for 1sec

Right arm
Right & Left arms
Very weak arm movements
Whiskers or mouth or nose
nothing

Electrical Stim. 3 mice
0.1mA-1mA
50Hz for 500ms or 1sec

Right arm
Right & Left arms
Very weak arm movements
Whiskers or mouth or nose
nothing

supplemental figure 1

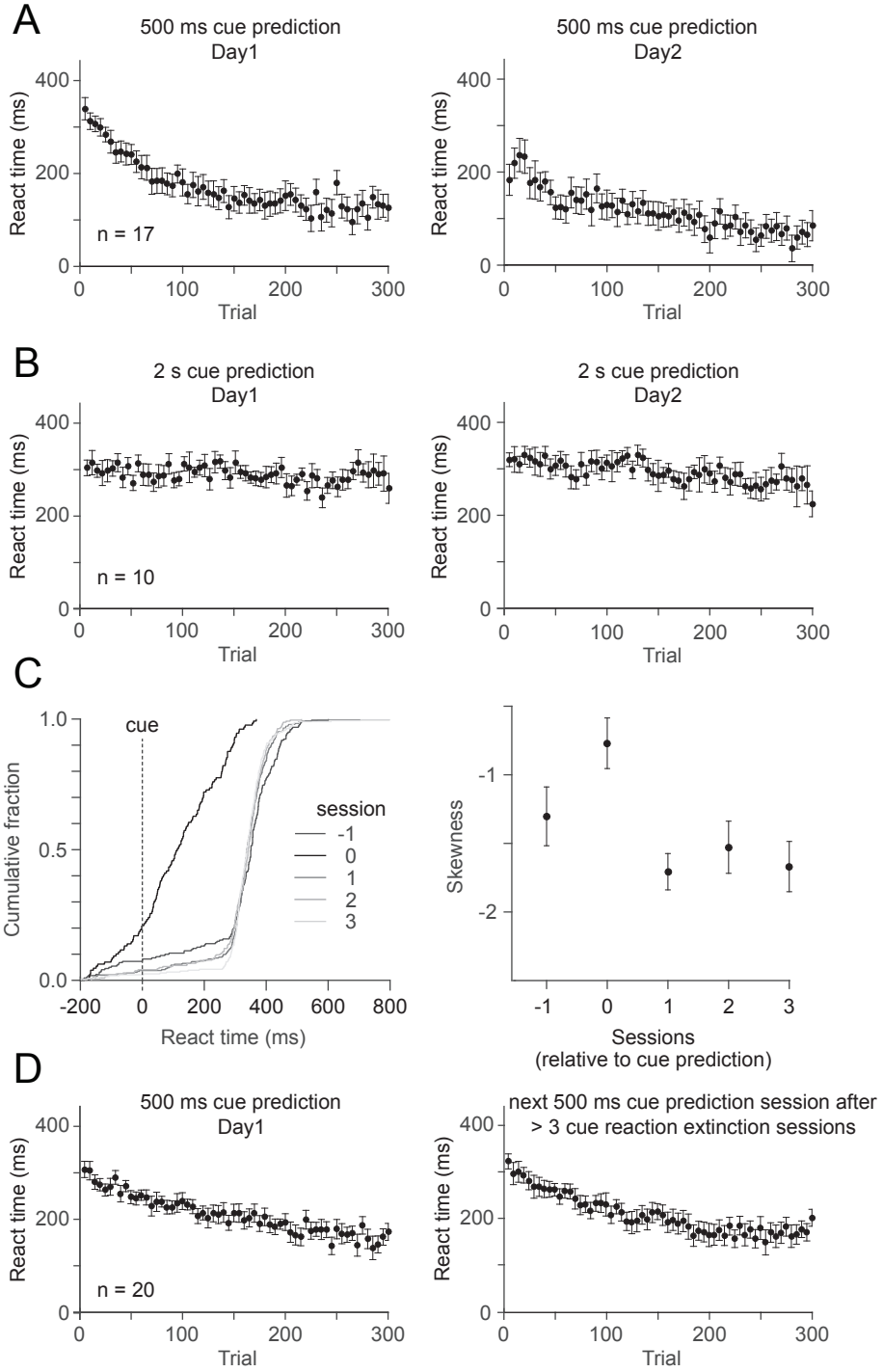

supplemental figure 2

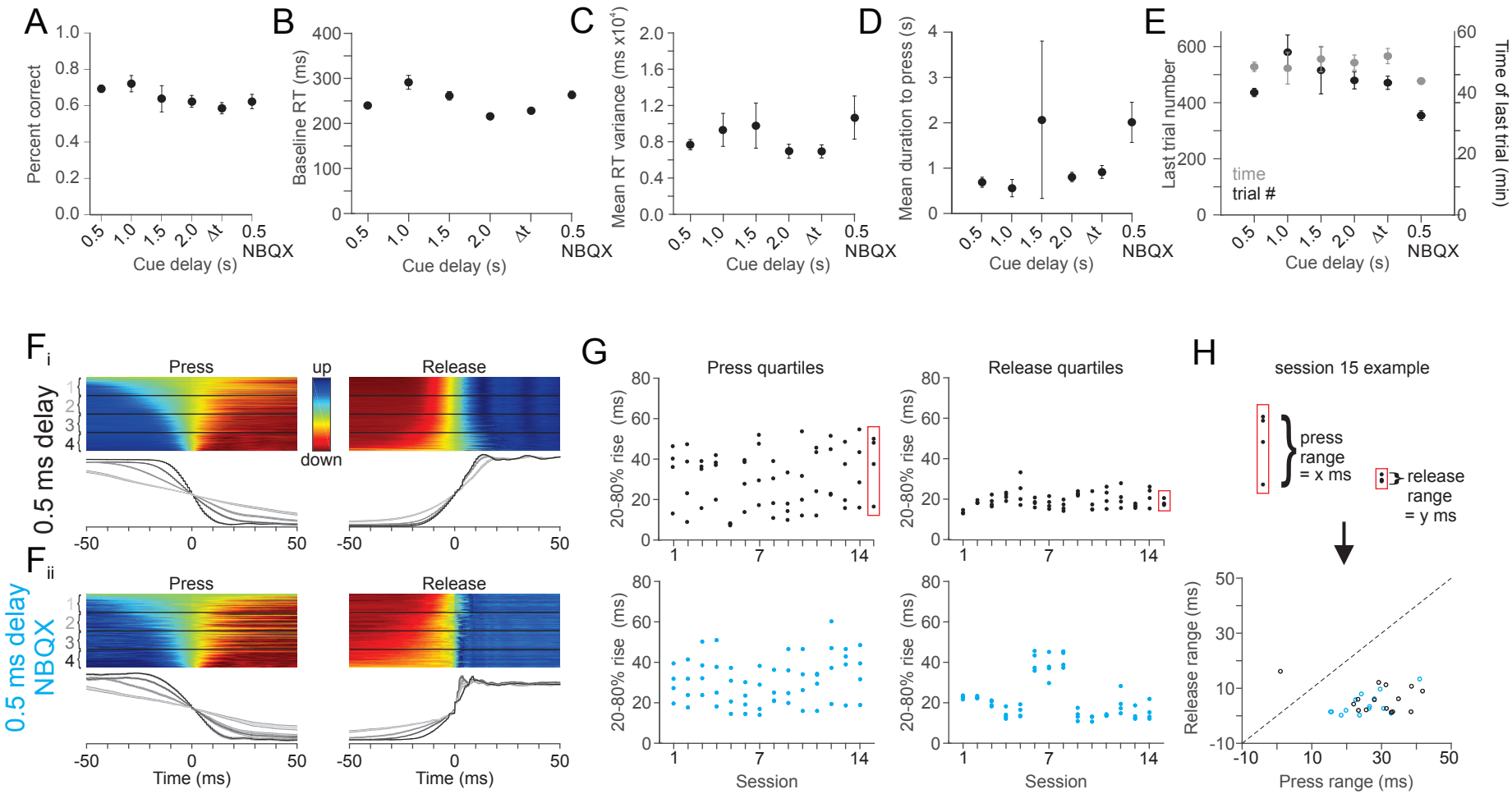

supplemental figure 3

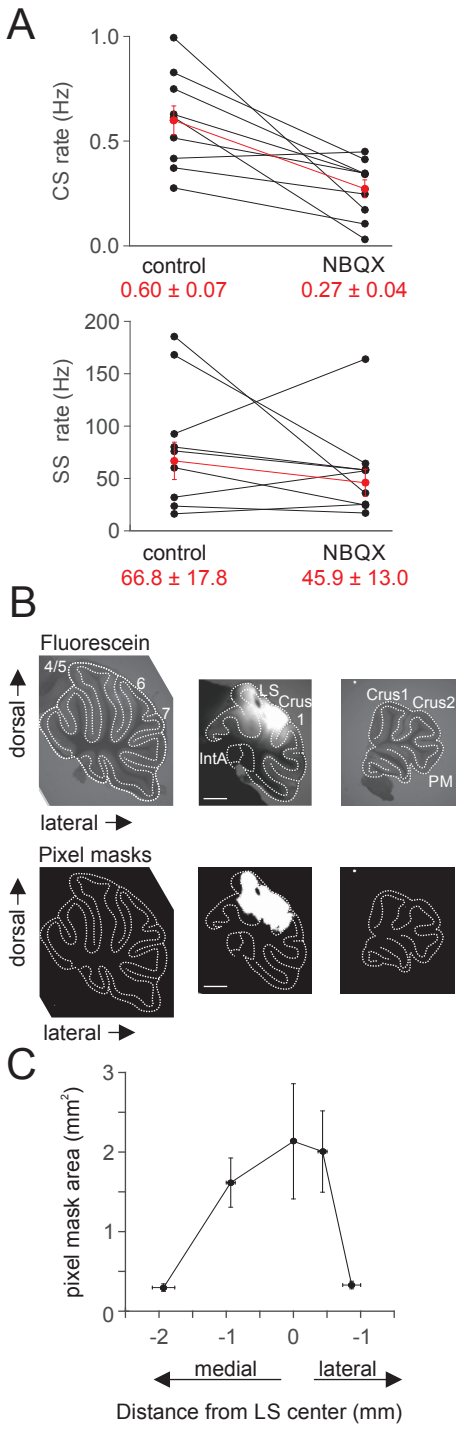

supplemental figure 4

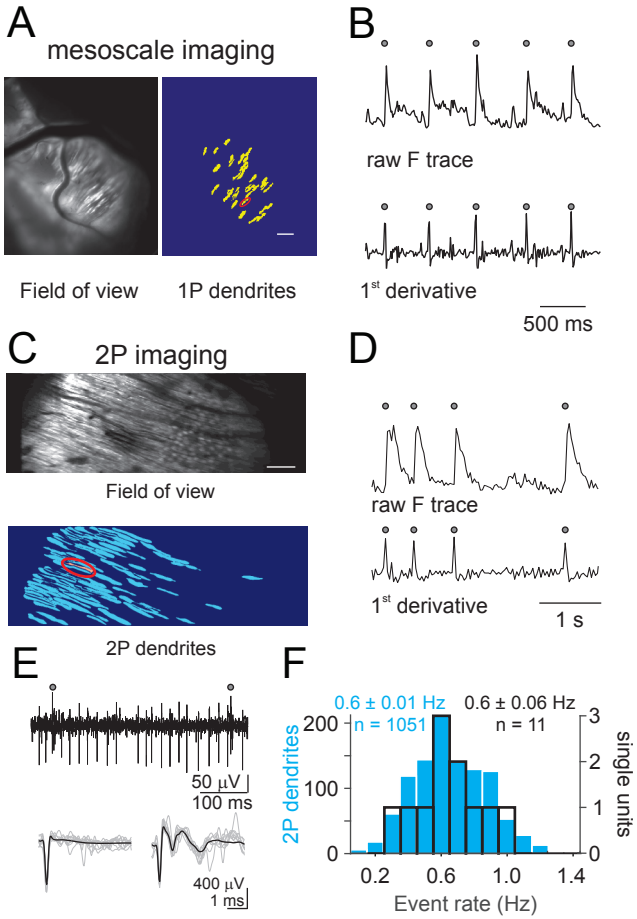

supplemental figure 5

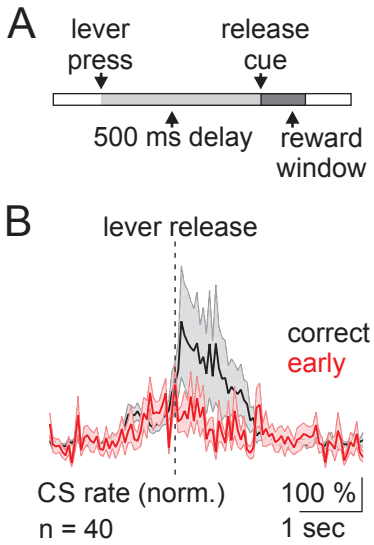

supplemental figure 6

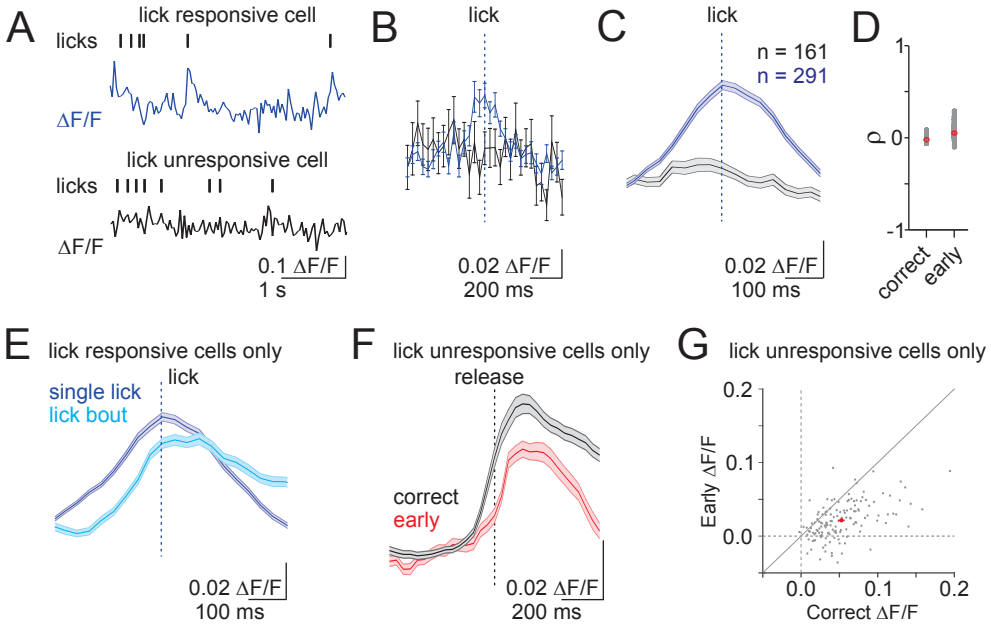

supplemental figure 7

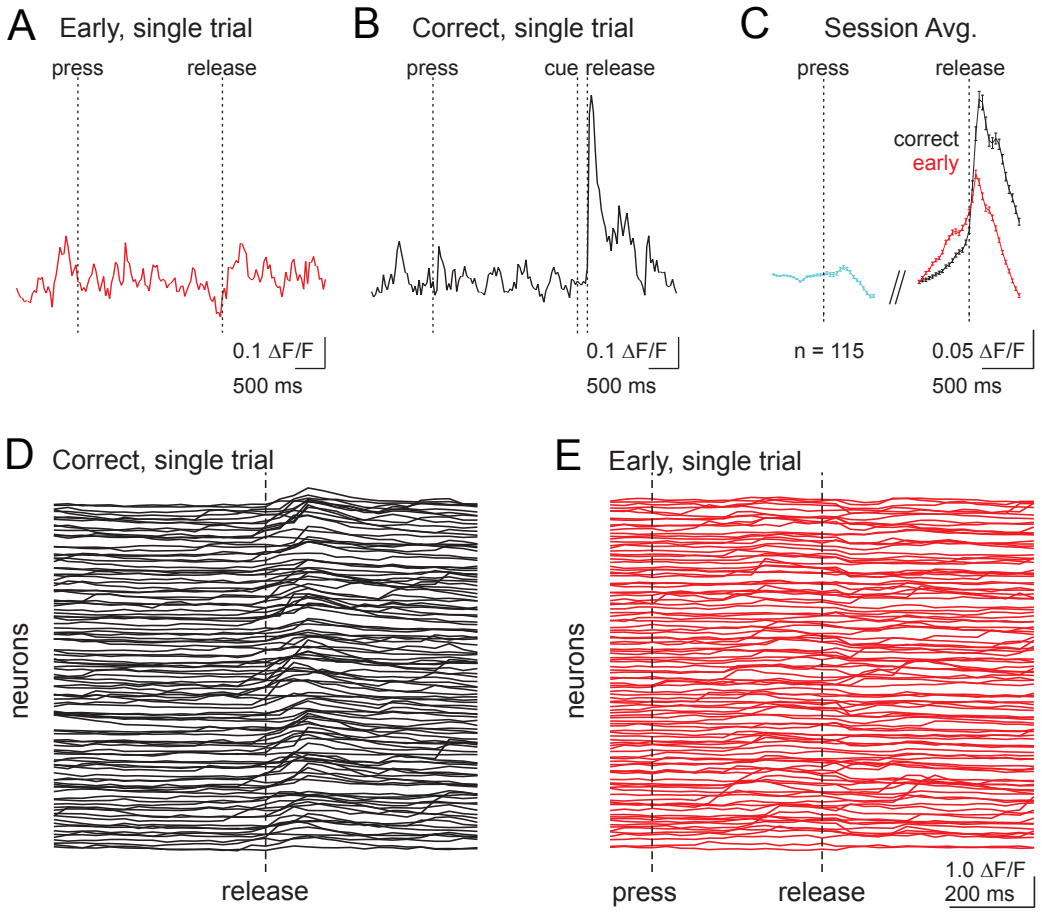

supplemental figure 8

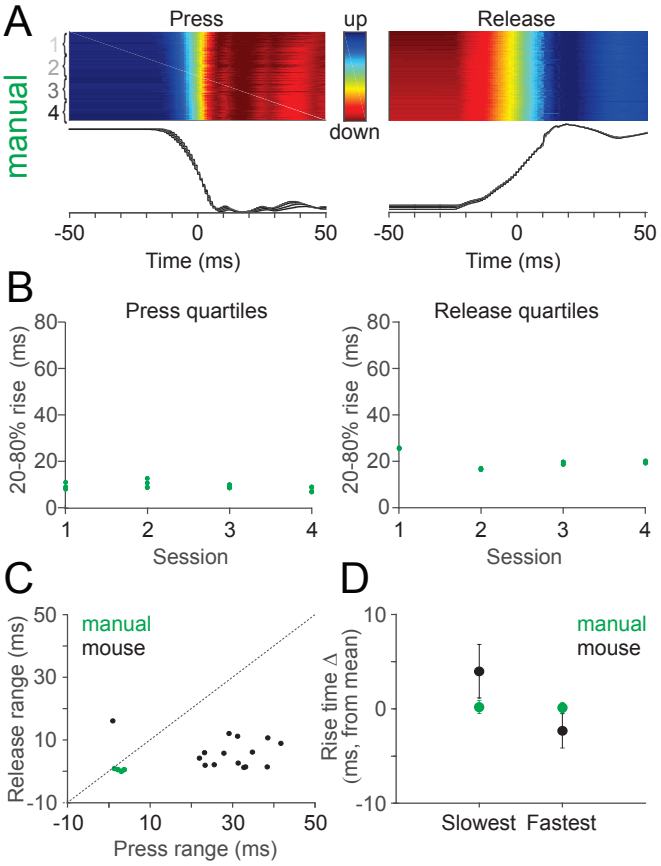

supplemental figure 9

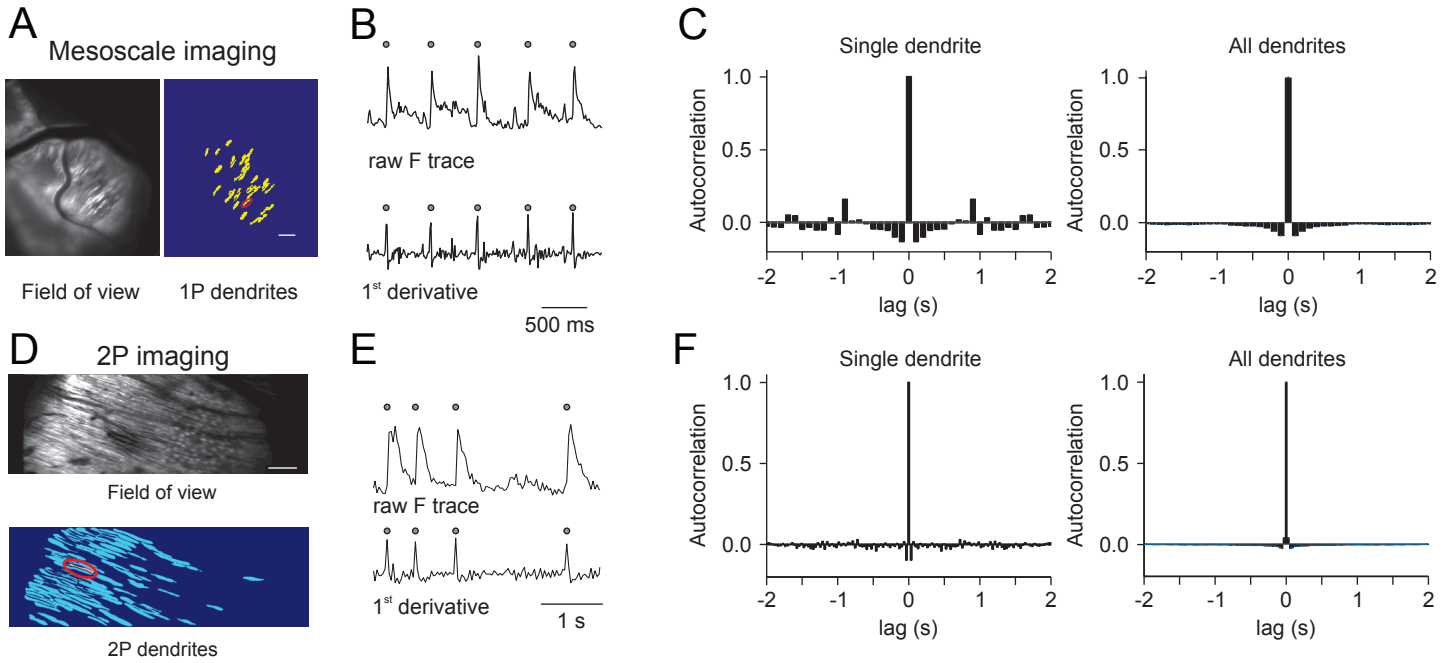

Reviewer Figure